Order Number 9009763

Optical refractive and reflective properties of resonantly absorbing medium

Mitwally, Kahil A., Ph.D.

City University of New York, 1989

U·M·I
300 N. Zeeb Rd.
Ann Arbor, MI 48106

OPTICAL REFRACTIVE AND REFLECTIVE PROPERTIES OF RESONANTLY ABSORBING MEDIUM.

BY

KAHIL A. MITWALLY

A dissertation submitted to the Graduate Faculty in Engineering in partial fulfillment of the requirements for the degree of Doctor of Philosophy, The City University of New York.

1989

This manuscript has been read and accepted for the Graduate Faculty in Engineering in satisfaction of the dissertation requirement for the degree of Doctor of Philosophy.

5/31/89
Date

Chair of Examining Committee

6/1/89
Date

Jacques E. Benveniste
Executive Officer

Professor S. Ahmed

Professor L. Roytman

Dr. D. Kokkinos

Supervisory Committee

The City University of New York

ACKNOWLEDGEMENTS

I would like to take this opportunity to acknowledge my deep appereciation to my thesis advisor: Professor Samir Ahmed for his patient guidance, continued encouragement, and numerous invaluable suggestions and discussions during the course of this research. I am also grateful to Prof. Aly Fathy and Prof. L. Roytman for their valuable theoretical assistance.

My thankfulness goes to my fellow graduate students for their assistance, providing laughter and sunshine during my stay at CCNY.

TO
MY WIFE SUZY
AND
MY SON AHMED

TABLE OF CONTENTS

Chapter 1		Page
	INTRODUCTION AND BACKGROUND	1
1.1	INTRODUCTION	1
1.2	BACKGROUND	5
1.21	Experimental Methods	5
1.2.2	Reflection at Normal Incidence-Measurement of Index of Reflection	5
1.2.3	Reflection at Oblique Incidence	7

Chapter 2

	Optical refractive and reflective properties of resonantly absorbing medium	24
2.1	Introduction	24
2.2	Theory	25
2.2.1	Background	25
2.2.2	Reflectance in terms of n and α	26
2.3	Reflectance in terms of α	28
2.4	Experimental	32
2.5	Comparisons of Theoretical Predicti and Experimental Results	36
2.6	Conclusion	49

Chapter 3

On the State of Polarization of a Reflected Beam from a Resonantly Absorbing Medium 50

3.1 Basic Parameters of Polarization 50

3.1.1 Introduction 50

3.2 Properties of polarization light 51

3.2.1 Basic definitions-liner Polarization 51

3.2.2 Elliptic Polarization 55

3.2.3 Polarization and Depolarization Factors 60

3.3 The State of Polarization 63

3.3.1 Introduction 63

3.4 Theory 64

3.4.1 General 64

3.4.2 r_p in the form A + J Ψ 65

3.5 Reflectance in Terms of α 67

3.6 Fractional Depolarization of the Reflected Beam 71

3.7 Experimental 73

3.8 Comparisons of Theoretical Predictions and Experimental Results 75

Appendix A 87

Appendix B 90

Reference 93

List of Figures

Number		Page
1.1	R-versus-Φ curves calculated using the optical constants .	11
1.2	Isoreflectance curves for R_p calculated using the optical constants	13
1.3	The effect of + 1 o/o erroe in the measurement of reflectance on the determination of n and k using method 1.	16
1.4	Curves of constant n and k as a function of R_p/R_s	18
1.5	Curves of constant n and k as a function of R_p and and R_s.	20
1.6	Curves of constant n and k as a function (a) of R_p/R_s and the pB angle and (b) of R_s and the pB angle (method 4 and 5, respectively).	23
2.1	Absorption spectrum of Rhodamine B in Ethanol	34
2.2	Experimental setup for reflection measurement	35
2.3	Reflectance R_p vs. λ for Rh B solution at angle of incidence $\phi = 29^o$	39
2.4	Reflectance R_p vs. λ for Rh B solution at angle of incidence $\phi = 54^o$	40
2.5	Reflectance Rp vs. λ for Rh B solution at angle of incidence ϕ = 75o	41

2.6	Theoretical predictions of reflectance Rp vs. angle of incidence ϕ at wavelengths λ = 514, 552, and 580 nm	43
2.7	Experimental measurements of reflectance Rp vs. angle of incidence ϕ at wavelengths λ= 514, 552, and 580 nm	44
2.8	Expansion of Fig 2.6 with the scale used in Fig. 2.7 to more readily distinguish between the data	45
2.9	Pseudo-Brewster angle ϕ_{pB} vs. λ	47
2.10	Reflectance at Brewster angles vs. λ	48
3.2.1	Orientation of the electric vector E at an instant of time, with respect to the plane of reference for a wave propagation along the z direction.	53
3.2.2	Linearly polarized plane electromagnetic wave.	54
3.2.3	Vibration ellipse for the electric vector.	58
3.2.4	Vaibration in the form of an elliptical vibration with phase difference.	59
3.7	Experimental setup for Depolarization measurement	74
3.8.1	Pseudo-Brewster angle ϕ_{pB} vs. λ	76
3.8.2	Fractional depolarization (D) of the reflected beam vs. angle of incidence ϕ at wavelength λ = 514 nm	79
3.8.3	Fractional depolarization (D) of the reflected beam vs. angle of incidence ϕ at wavelength λ = 552 nm	80
3.8.4	Fractional depolarization (D) of the reflected beam vs. angle of incidence f at wavelength l = 580 nm	81

3.8.5 Fractional depolarization (D) of the reflected beam vs. l for Rh B solution at angle of incidence f = 29o 83

3.8.6 Fractional depolarization (D) of the reflected beam vs. l for Rh B solution at angle of incidence f = 54o 84

3.8.7 Fractional depolarization (D) of the reflected beam vs. l for Rh B solution at angle of incidence f = 75o 85

A.1 The integration contour used to drive the real part (n) of the complex refractive index (N)

CHAPTER 1
INTRODUCTION AND BACKGROUND

1.1 INTRODUCTION:

High absorption coefficients encountered in the fundamental absorption regions make transmission measurements impractical in many cases. Thus most of the work reported in the literature [1-5] involve the analysis of normal incidence reflectance data. Such data can be processed using the Kramers-Kronigs relations to yield the optical constants of an absorbing medium.

The index of refraction n and the extinction coefficient k of an isotropic material represent the real and imaginary components of the complex index of refraction N = n - ik. At a given wavelength they may be obtained by direct methods or inferred from photometric or polarimetric measurements. A number of methods [1-9] exist for extracting n and k from specular reflectance measurements at both normal and oblique incidence. Humphreys-Owen [4] lists nine methods by which n and k can be deduced from reflectance measurements at oblique incidence. These methods are divided into two classes: (1) two reflectance measurements at one angle of incidence or one reflectance measurement at each of two angles of incidence, and (2) one reflectance measurement at any angle of incidence and measurement of a special angle of incidence satisfying certain specific conditions. This special angle is the

Brewster angle. Its value, ϕ_B, for a lossless medium, is related to the indices of refraction of the two media, n1, and n2, by the simple equation: $\tan \phi_B = n2 / n1$. At this angle the component of specular power reflectance, RP, of a light beam linearly polarized parallel to the plane of incidence drops to zero. For a lossy medium, however, it has been observed by many workers that RP always has a minimum value, but it is not zero. The angle at which this minimum occurs is therefore called the pseudo-Brewster (PB) angle.

Most of the work reported in this field has focused on measuring the values of the PB angles and the corresponding reflectance for each angle at the wavelengths of interest.

In the work reported here, first, we examine the reflection of a polarized collimated monochromatic light beam from an absorbing medium (an organic dye solution) with a known and clearly defined resonance absorption spectrum, rather than trying to extract its absorption coefficient from the measured reflectance data.

To compare the experimental results with theory, the Fresnel reflectivity equations [10] combined with the Kramers-Kronig relations [11] were used to predict the reflectance in terms of the known absorption coefficient, angle of incidience, and the wavelength.

Second, we explore depolarization effects in specular reflections from resonantly absorbing media, including examinations

of why the reflection component, R_p, at the pB angles never reaches zero for a lossy medium, in contrast to the exactly zero reflectance at the Brewster angle, for a lossless medium. In the work reported here, we focus our attention on the nature and the state of polarization of the reflected beam (assumed to be " P" polarized before reflection) particularley at the PB angles, rather than measuring the reflectance and the pB angles. The Fresnel reflectivity equqtions [10] combined with the Kramers-Kronig trasformations [11] were used to predict the state of polarization of the reflected beam. These properties are examined in the context of reflections of a collimated monochromatic light beam at the planar interface of the medium and the air.

It was found that, at all the PB angles for all wavelengths of interest, the reflected beam is totally depolarized (in a direction normal to the plane of incidence i.e. it represents the component of the specular reflection perpendicular to the plane of incidence, Rs) explaining the fact why RP never drops to zero at the PB angles.

Using the tunable polarized output of a cw dye laser to provide the collimated monochromatic beam, surface reflections measurements at the planar interface of the absorbing medium and air were made for a variety of situations, including Brewster's angle in the spectral vicinity of the resonance wavelength. An ethanolic solution of Rhodamine B, an organic laser dye luminofor with a well defined resonance absorption spectrum, was chosen as the absorbing medium.

The polarization of the reflected beam was measured using rotating polarizers. The experimental results generally confirm the theoretical predictions, and demonstrate that at all the PB angles the reflected beam is totally depolarized.

1.2 BACKGROUND:

1.2.1 Experimental Methods:

The optical constants of an isotropic material are the index of refraction n and extinction coefficient k. They are the real and imaginary components of the complex index of refraction N = n - jk. They can be measured at a given wavelength by direct methods or inferred form photometric or polarimetric measurements. A number of methods exist for extracting n and k from specular-reflectance measurements at both normal and oblique incidence and for semi-infinite media as well as layers on substurates. Here we will discuss the most useful methods for obtaining n and k and the problem encountered in applying these methods.

1.2.2 Reflection at Normal Incidence-Measurement of Index of Reflection.

The reflection of a collimated light beam is governed by the Fresnel coefficients [10]

$$r_p = \frac{\epsilon \cos\phi - (\epsilon - \sin^2\phi)^{1/2}}{\epsilon \cos\phi + (\epsilon - \sin^2\phi)^{1/2}}$$

$$r_s = \frac{\cos\phi - (\epsilon - \sin^2\phi)^{1/2}}{\cos\phi + (\epsilon - \sin^2\phi)^{1/2}} \qquad (1.2.1)$$

$$\varepsilon = \varepsilon' + j\varepsilon'' \qquad (1.2.2)$$

where p and s identify the linear polarizations parallel and perpendicular to the plane of incidence, respectively. f is angle of incidence, and

$$\varepsilon = \varepsilon_1 / \varepsilon_o \qquad (1.2.3)$$

is the complex ratio of dielectric constants of the two media defined as:

$$\varepsilon = \varepsilon' + j\varepsilon''$$

At normal incidence the two components of reflection are indistinguishable and, for nonabsorbing media, the equations may be reduced to

$$R = (n-1)^2/(n+1)^2. \qquad (1.2.4)$$

Since;

$$N^2 = \varepsilon = \{n^2 - k^2\} + j2nk = a + jb \qquad (1.2.5)$$

Unlike the generalized coefficients, this equation can be solved for n as

$$n = (1+R^{0.5})/(1-R^{0.5}) \qquad (1.2.6)$$

The values of n of transparent media in the vacuum ultraviolet (VUV) usually range from 1.3 to 2.0. Over this range the absolute error in determining n from reflectance measurements is approximatly 10 times the absolute error in measuring R.
Thus n is sensetive to small errors in R and the accuracy of the method makes it suitable only for determining provisional values to two significant figures at best.

This simple method may be used for any material that is transparent in the VUV and can be polished or cleaved to give specularly reflecting surface. Precautions must be taken to measure reflectance from the first surface only. Reflections from the second surface can be eliminated by making the sample wedge shaped or can be suppressed by grinding the second surface and blackening it.

1.2.3. Reflection at Oblique Incidence:

Humphreys-Owen [4] lists nine methods by which n and k can be deduced from reflectance measurements at oblique incidence. These methods are divided into two classes:

(1) two reflectance measurements at one angle of incidence or one reflectance measurements at each of two angles of incidence and
(2) one reflectance measurement at any angle of incidence and measurement of a special angle of incidence capable of supplying the necessary second measurement. There are two special angles:

1- the principal angle of incidence, which must be determined by polarimetric methods and so it will not be discussed, and
2- the Brewster, or pseudo-Brewster(pB), angle. The Brewster angle is defined only in terms of dielectric media and is given by

$$n = \tan \phi_B \qquad (1.2.7)$$

At this angle $R_p = 0$. As k increases, R_p always has a minimum value, but it is not zero. The angle at which this minimum occurs is the pB angle and, if

$$k > 0, \phi_{pB} > \phi_B .$$

Humphreys-Owen's list has been rearranged as follows:

Class 1

Method 1 Reflectance at two angles of incidence using natural or polarized radiation; sometimes referred to as *the* reflectance versus-angle of incidence method

Method 2 The ratio R_p / R_s at two angles of incidence

Method 3 R_s and R_p at one angle of incidence

Class 2

Method 4 Pseudo-Brewster angle and R_s or R_p at that angle

Method 5 Pseudo-Brewster angle and R_p / R_s at that angle

Method 6 Pseudo-Brewster angle and R_s, R_p or R_p / R_s at any other angle of incidence

In principle, only two measurements are required, but, because of possible errors in the measurements, a redundancy of measurements is more useful and will give an indication of the errors involved in determining n and k.

Although these methods can be used at any wavelength, their sensitivities to errors in measurements of reflectance, of the angles involved, or of the state of polarization are functions of both n and k, as well as the angle of incidence and the state of polarization. Thus there may be parts of the n, k plane, angles of incidence, and state of polarization, for which the lack of sensitivity reduces their accuracy to unacceptable values.

Since the sensitivities of the methods are dependent on n, and k, hence on the shape of the R-versus-f curves, a collection of these curves is shown in fig. (1.1)[12] for reference during the ensuing discussion. The large numbers give the values of n and k used in calculating a particular set of curves. These values covers the range of n and k most likely to be encountered in the VUV. The small numbers along the abscissa and ordinate show the angle of incidence and percent reflectance, respectively. The upper curve is always Rs, the lower curve Rp, and the curve between Ra. Generally, for a given n, as k increases the reflectance at normel incidence increases, the change in R with f becomes small, especially for Ra, except at the pB angle, and the pB angle becomes large. For a given k, as n increases the reflectance at normal incidence decreases, the change in R with f becomes more pronounced, especially for Rp, and again the pB angle

becomes larger. The value of Rp at the pB angle appears to be zero for n > 1.3 and k = 0.3. This is not so, but the values are extremely small.

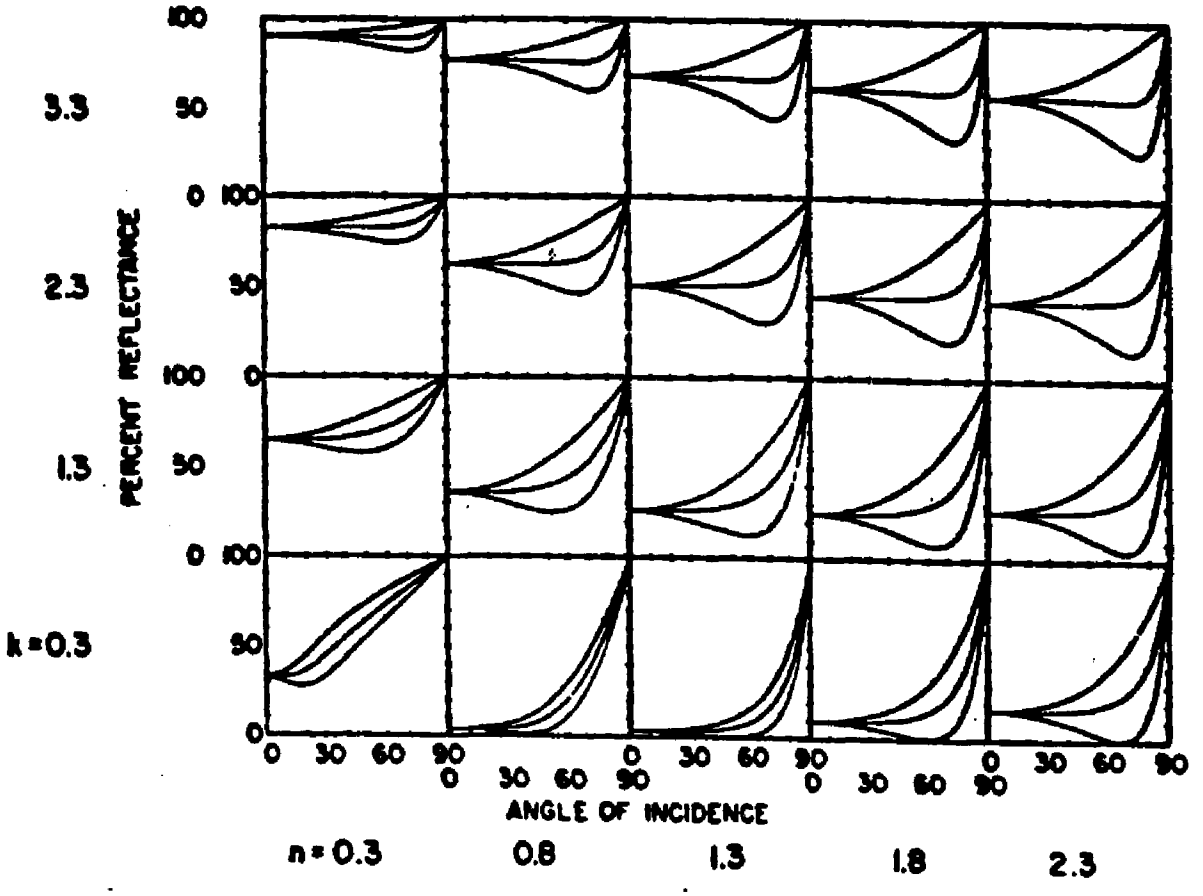

FIG. 1.1 R-versus-ϕ curves calculated using the optical constants shown by the large numbers. The small numbers shown on the abscissa and ordinate are the values of ϕ and R, respectively.

Method 1:

The sensitivity of this method is most easily investigated by means of isoreflectance curves. An isoreflectance curve is the locus of points in the n, k plane corresponding to a given value of R for a specific value of ϕ. If isoreflectance curves are plotted for perfect data, i.e., reflectance values calculated using the Fresnel formula, an insight into the sensitivity of the method can be obtained. Fig. (1.2) [12] show such a set of curves for the parallel component covering that part of n, k plane

$$0.3 < n < 2.3 \text{ and } 0.3 < k < 3.3.$$

An indication of the sensitivity is the angle of intersection of the isoreflectance curves. If there is an error in the reflectance, the isoreflectance curve will be shifted parallel to its self by an amount depending on the magnitude of the error and in a direction depending on its sign. Thus, if two curves intersect at a small angle, a slight displacement of one with respect to the other may shift the intersection point by a large amount. Such a displacement could be due either to an error in measuring R or an error in measuring f. The figure indicates that for n = 0.3, the sensitivity with respect to k decreases as k increases. Thus for small n and k > n, the R-versus-f method can provide reasonable values, e.g., Al, Mg, etc., usually have small n and k > n. For example, at 1216 A, Al has n 0.06 and k 1.0.

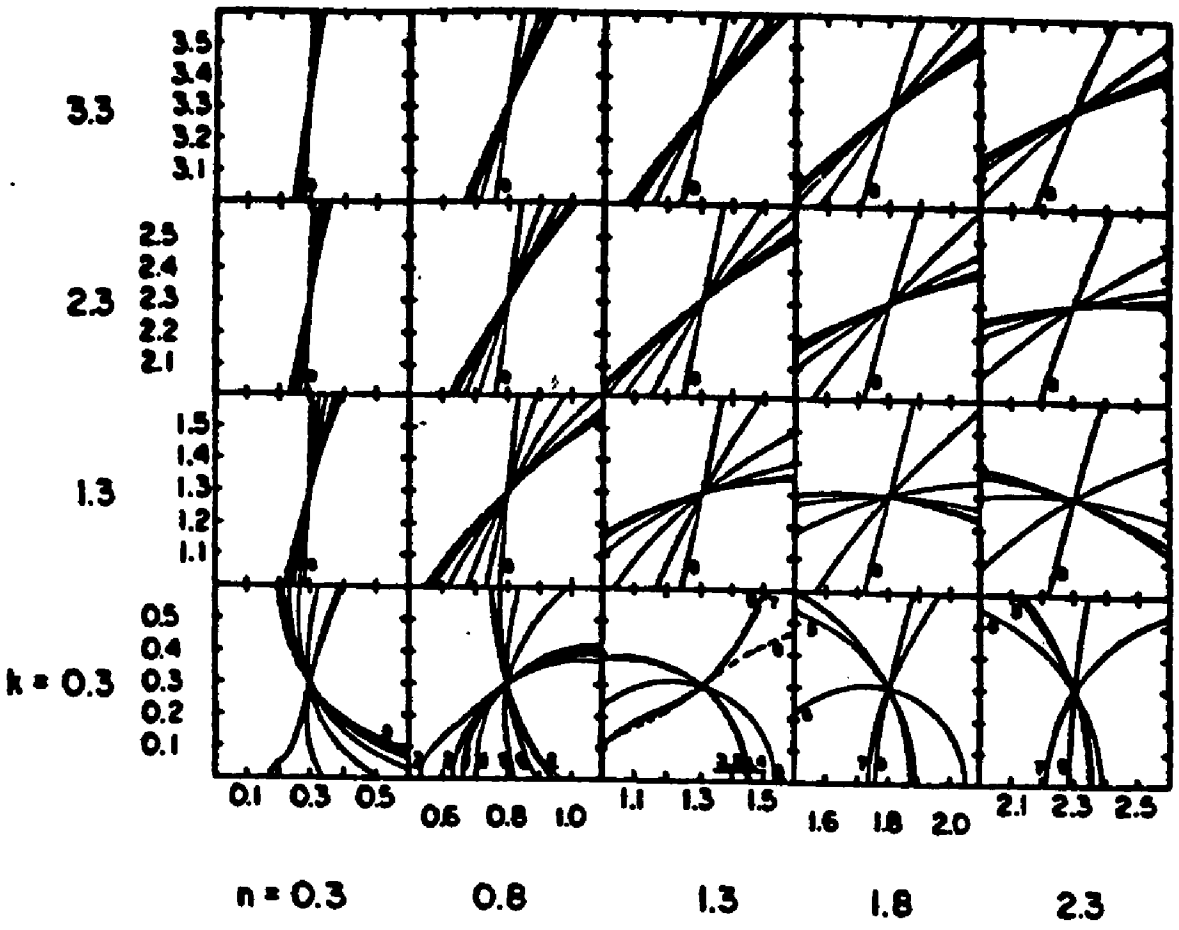

FIG. 1.2 Isoreflectance curves for R_p calculated using the optical constants shown by the larger numbers. The small numbers used for the abscissa and ordinate show the scale in the n, k plane. The numeral 8 designates the isoreflectance curve corresponding to 80°. The other curves are for angles of incidence 70, 60, through 10°. The curves usually occur in descending order; when they do not, each curve is labeled with a single digit to avoid confusion (method 1)

For n > 0.3, the isoreflectance curves for small angles of incidence are more nearly parallel than those for the larger angles. Thus, the sensitivity is greatest if measurements are made at the larger angles of incidence. For n = 0.3, however, the maximum sensitivity for small k is obtained using small angles and as n increases, maximum sensitivity is shifted only slowly to larger angles. Generally, the angles with which maximum sensitivity is obtained are those angles at which the curvature in R is maximum, which is not necessarily the angles at which R changes most rapidly with f. Similar sets of isoreflectance curves have been calculated for Rs and Ra[12].

Although the curves in Fig. 1.2 furnish an idea of the sensitivity of the method, the accuracy of the method can only be found by using false data.

By adding positive and negative errors to perfect reflectance data, the magnitude of the displacement of the isoreflectance curves can be obtained and the accuracy of the method determined. Hunter [12] has investigated the accuracy of method 1 using angles of incidence of 20^o and 70^o. His results are shown in Fig. 1.3 for both Rp and Ra. The blackened parallelopipeds represent the error in determining n and k for $\pm$ 1 o/o erroes in measuring the reflectance. The parallelopipeds correspond to the values of n and k shown in large numbers. Lines connect the extermities of these parallelopipeds to indicate the magnitude of the errors at intermediate points. The

magnitude of the errores is in keeping with the sensitivity as discussed in connection with Fig. 1.2. For example, for small n (0.3), the error in n as k increases grows comparatively slowly, but the corresponding error in k becomes large quite rapidly because the parallelopipeds are almost parallel to the k axis. As n increases and for large k, the long axis of the parallelopipeds rotates in a clockwise direction so that the error in determining n increases while that for k decreases. It is evident that Rp is more tolerant of errors than Ra.

In using the R-versus-ϕ method it is not necessary to know the actual R values[12]. The fact that reflectance is defined as the ratio of the reflected intensity at angle ϕ to the incident intensity is equvalent to normalizing the reflected intensity at angle ϕ to the reflected intensity at 90^{o} angle of incidence, which is defined as unity. For use in the R-versus-ϕ method, normalization can be done at any angle of incidence and is referred to as oblique normalization. Field and Murphy [13] have puplished an analysis of the R-versus-ϕ method for oblique normalization. For oblique normalization the angle between the isoreflectance curves may not be a good indicator of sensitivity, and one should plot known errors in the obliquely normalized reflectance values to get a correct indication of sensitivity. Oblique normalization has no advantages over the usual mode of normalization and is only used when the physical arrangement of the reflectometer makes measurement of the incident intensity impractical.

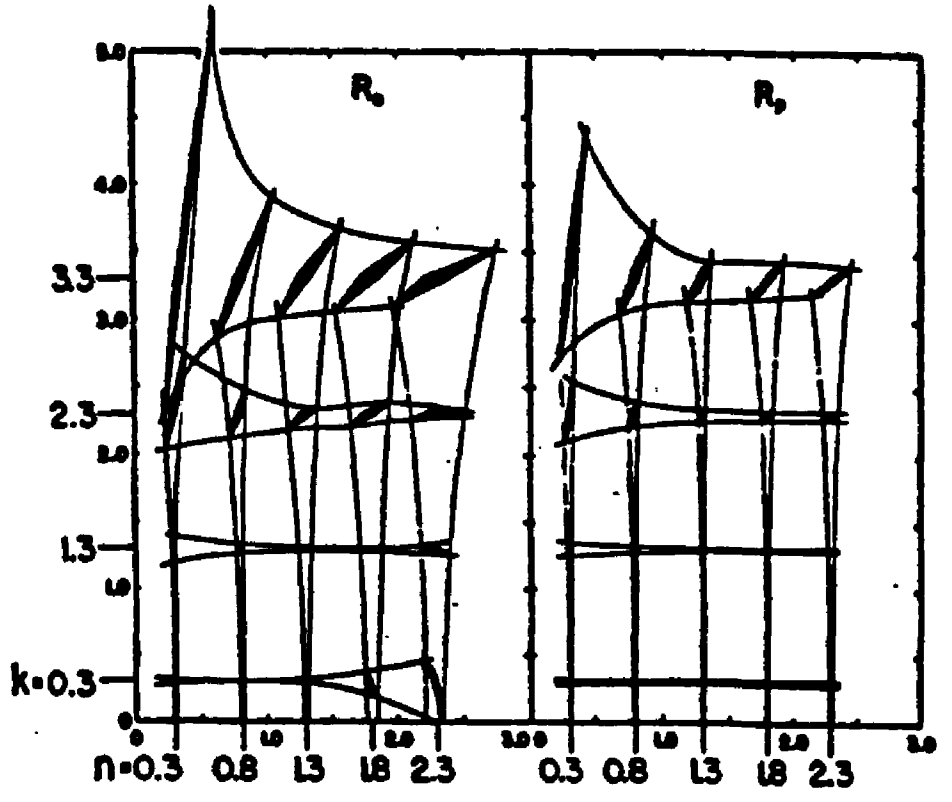

FIG. 1.3 The effect of + 1 o/o error in the measurement of reflectance on the determination of n and k using method 1. The angles of incidence are 20 and 70°

Method 2:

Figure 1.4 shows two sets of curves for the ratio Rp / Rs. To the left is a set for small angles of incidence and to the right a set of large angles. According to Humphreys-Owen, an indication of the sensitivity is the spacing between contours- if the spacing is large, the sensitivity is good and vice versa. As suming that his assertion is correct, the large-angle contours are obviously not useful if n and k are large but might be used to obtain good values if n and k are small. The small-angle contours are only useful if n and k are small. Humphreys-Owen showed a limited set of contours of Rp/Rs for 80^{o} and 60^{o}, and a more extended, calculated set indicates that these two angles may be more useful than those shown here for larger values of n and k.

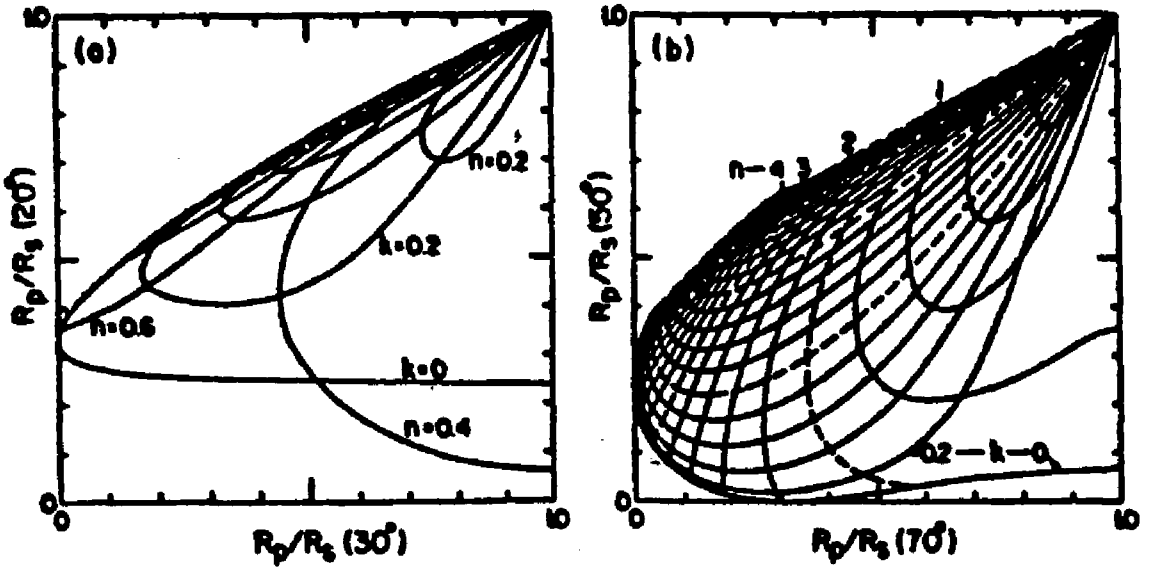

FIG. 1.4 Curves of constant n and k as a function of R_p /R_s for (a) small (30-20°) and (b) large (70-50°) angles of incidence. Δn and Δk are each 0.2. Curves for integer n and k values are dashed (method2)

Method 3:

Figure 1.5 shown two sets of curves for Rs and Rp at both 20^o and 70^o angles of incidence. Judging from sets of curves obtained for other angles of incidence, these two angles are the most useful. For 20^o angle of incidence, the curves of conestant k are spaced 0.01 apart from $k = 0$ to $k = 0.1$. The next k contour is for $k = 0.2$ and thereafter $\Delta k = 0.2$. The n contours have $\Delta n = 0.1$. The dotted line is the contour of $n = 0.364 = \tan 20^o$. This set of curves might be useful for $n < 0.5$ and $k < 0.4$.

The set of curves of 70^o is less useful for small n and k but more useful for larger values. For this set $Rp = 0$ when $n = 2.747 = \tan 70^o$. Both Δn and Δk are 0.2 for this set.

The envelope of the 20^o contours consists of the curves $k = 0$ and, ultimately, the curves for large n values. The 70^o contours are enveloped by the two curves for $k = 0$, which coincide at $Rs = Rp = 0$. At 45^o, where $Rp = Rs^2$ for any n and k, the envelope is compressed to a line that has the form of a parabola.

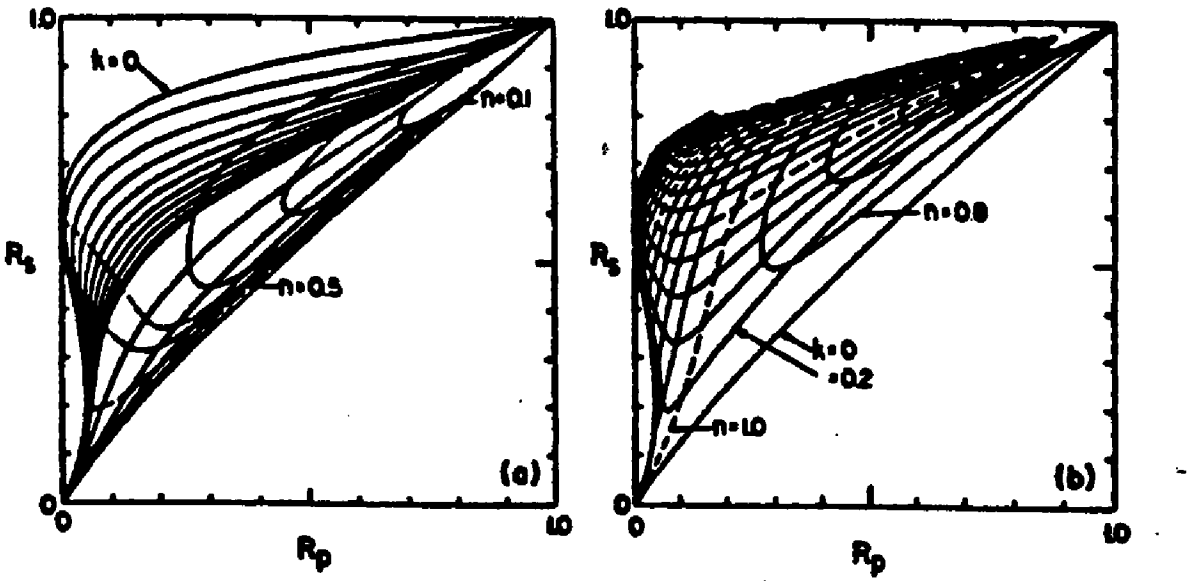

FIG. i.5 Curves of constant n and k as a function of R_p and R_s for (a) small (20°) and (b) large (70°) angles of incidence. For (a) Δk is 0.01 for $0 < k < 0.1$; otherwise Δk is 0.2. Δn is 0.1 and the curve for $n = 0.5$ is dashed. The dotted line corresponds to the value of n for the Brewster angle, $n = 0.364$. Φpr (b) $\Delta k = \Delta n = 0.2$. Curves for integer n and k values are dashed (method 3)

Method 4 and 5:

Figures 1.6 shows sets of curves for Rp/Rs (method 4) and Rs (method 5) versus the pB angle. The Rp/Rs set favors small values of n and k and the Rs set favors somewhat larger n and k. Not that the Rs curves can give double values. For example, if the pB angle is 15^{o} and Rs = 0.56, k would be 0.3 but n could be 0.2 or 0.3. Thus, the region with double values is not useful. Contours for Rp-versus-pB angle are similar to those for Rp/Rs.

According to Humphrey-Owen, method 6 gives no advantages over the other methods.

In order to obtain quantitative data on the accuracy of methods 2-5, it is necessary to plot the contours for $R \pm \Delta R$, or $pB \pm \Delta pB$, which has not been done. The existance of large spacing between the contours suggests but does not guarantee small displacements of the contours when errors are introduced Humphrey-Owen points out that R_p, at the pB angle, can be quit small; thus, there may be a large error in measuring it. Furthermore, the minimum in R_p at the pB angle is usually broad, so accurate location of the angle may be difficult.

If method 2 or 5 is to be used, normalization to get acual reflectance values is unnecessary.

The equation for R_p can be manipulated to obtain the pB angle intermes of n and k[4]. It is given below,

$$2(p^2 + q)v^3 + p^2(p^2-3)v^2 - 2p^4v + p^4 = 0,$$

where

$$p = n^2 + k^2, \qquad q = n^2 - k^2, \qquad v = \sin^2 \phi_B$$

The experimental values for n and k obtained from the curves can be substituted in the formula to help verfiy the correctness of the results.

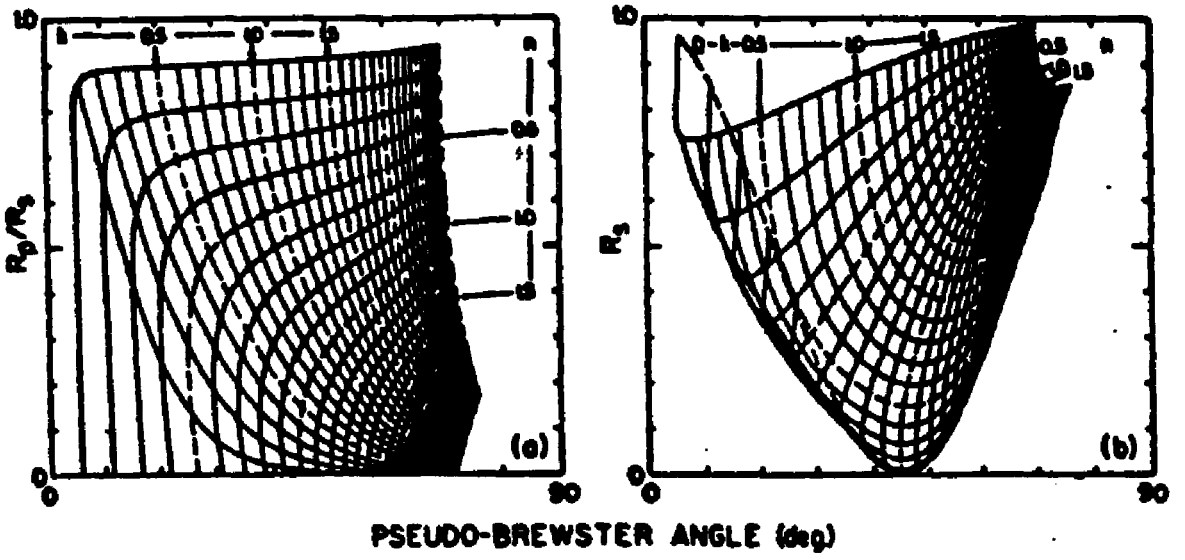

FIG. 1.6 Curves of constant n and k as a function (a) of R_p/R_s and the pseudo-Brewster (pB) angle and (b) of R_s and the pB angle (method 4 and 5, respectively). $\Delta n = \Delta k = 0.1$ and curves for integer and half -integer; n and k values are dashed.

Chapter 2

Optical refractive and reflective properties of resonantly absorbing medium.

2.1. INTRODUCTION

Experiments on the reflection of polarized monochromatic laser light at the planar interface of resonantly absorbing medium and the air were made for a variety of situations, including Brewster's angle in the spectral vicinity of the resonance wavelength. An ethanolic solution of Rhodamine B, an organic laser dye luminofor with a well defined resonance absorption spectrum, was chosen as the absorbing medium. The tunable polarized output of a cw dye laser was used to provide the collimated monochromatic beam. To compare the experimental results with theory, the Fresnel reflectivity equations combined with the Kramers-Kronig relations were used to predict the reflectance in terms of the known absorption coefficient. The experimental results generally confirm the theoretical predictions.

2.2. THEORY

2.2.1 BACKGROUND

In this section, the Fresnel reflectivity equation for the P-polarized beam (r_p) is expressed in a simple form and used to relate the intensity (or power) reflectance of a monochromatic collimated light beam at the planar interface between a transparent medium of incidence (usually air, $\varepsilon_0 = 1$) and an absorbing medium of refraction (ε_1 complex) in terms of the absorption coefficient (α) of the medium, the real part (n) of the complex refractive index of the absorbing medium, the angle of incidence (ϕ), and the wavelength of the incident beam.

Then, using the Kramers-Kronig relationships, an analytical expression for the real part of the complex refractive index is obtained in terms of the absorption coefficient (i.e. the imaginary part of the complex refractive index of the absorbing medium). This result is then combined with the general reflectance expression of step 1, to predict the reflectance of an absorbing medium at any given wavelength, solely in terms of the absorption coefficient of the medium at that wavelength and the angle of incidence.

2.2.2 REFLECTANCE IN TERMS OF n and α

The reflection of a collimated light beam is governed by the Fresnel coefficients [10] see appendix A

the reflectance for the P polarized beam, $\Re_p = r_p \overset{*}{r}_p$, can be expressed in the form:

$$\Re_p = \frac{a^2 + b^2 + Z^2 - 2|Z\{a\cos(\theta/2) + b\sin(\theta/2)\}|}{a^2 + b^2 + Z^2 + 2|Z\{a\cos(\theta/2) + b\sin(\theta/2)\}|} \tag{2.1}$$

We next relate the real and imaginary quantities, a and b, to the absorption coefficient of the medium. The complex refractive index , N, is defined by: N = n + jk, where the imaginary part, k, is related to the absorption coefficient, α by:

$$k = \frac{c}{2\omega}\alpha(\omega) \tag{2.2}$$

where c is the speed of light in free space and ω is the angular frequency.

The complex refractive index, N, is also related to the dielectric constant of the medium by the relation:

$$N^2 = \varepsilon = \{n^2 - k^2\} + j2nk = a + jb \tag{2.3}$$

combining Eqs. (A.2), (2.2) and (2.3) gives:

$$a = n^2 - \frac{c^2}{4\omega^2}\alpha^2(\omega) \qquad b = n\frac{c}{\omega}\alpha(\omega) \tag{2.4}$$

This means that all the terms in Eq (A.3) are now available in terms of n and α (as well as ω, c, and ϕ).

2.3 REFLECTANCE IN TERMS OF α

We now turn to the second part of the problem to find $n(\omega)$ in terms of the absorption coefficient $\{\alpha(\omega)\}$, so that the solution of Eq.(2.1) can be obtained in terms of the absorption coefficient only.

Since the imaginary part $\{k(\omega)\}$ of the complex refractive index is given by Eq. (2.2) in terms of α and ω, using the Kramers-Kronig relations, the real part $\{n(\omega)\}$ can also be determined in terms of α and ω within an arbitrary constant (n_1) which can be determined from the specific physical conditions. The Kramers-Kronig relation for the real part $n(\omega)$ is given by [14]:

$$n(\omega') = n_1 + \frac{1}{\pi} P.V. \int_{-\infty}^{\infty} \frac{k(\omega)}{(\omega - \omega')} d\omega \qquad (2.5)$$

where P.V. means the Cauchy principal value.

It is important to stress the generality of the relation of Eq. (2.5). It requires only boundedness and causality [15]. These conditions are necessarily fulfilled by virtue of the fact that the polarization of a wave cannot antecede the arrival of the disturbing electric field that produces it [16].

Rewriting Eq. (2.5) in terms of α (Eq. 2.2) gives:

$$n(\omega') = n_1 + \frac{c}{2\pi} P.V. \int_{-\infty}^{\infty} \frac{\alpha(\omega)}{\omega(\omega - \omega')} d\omega \qquad (2.6)$$

To obtain reflectance in the vicinity of the absorption resonance, using Eq. (2.1), it is first necessary to evaluate the integration of Eq. (2.6) over the spectral range of interest, and then substitute the results into Eq. (2.1). To evaluate the integration in Eq. (2.6), two possible approaches could be used. The first would be to carry out a numerical integration using the actual measured absorption lineshape (Fig. 2.1).

The second approach is to assume a Lorentzian approximation for the absorption lineshape in the vicinity of the peak, and to analytically integrate Eq. (2.6) to get an analytical expression for $n(\omega)$. For this approach, we assume a Lorentzian function for the absorption coefficient $\alpha(\omega)$, given by:

$$\alpha(\omega) = \frac{\alpha(\omega_0)\gamma^2}{(\omega - \omega_0)^2 + \gamma^2} \qquad (2.7)$$

where:

$\gamma = (\Delta\omega / 2)$, and $\alpha(\omega_0)$ is the absorption coefficient at resonance Substituting Eq. (2.7) into Eq. (2.6) and carring out the integration we get (see appendix):

$$n(\omega) = n_1 + \left\{ \frac{c(\omega_0^2 - \omega\omega_0 - \gamma^2)}{2\gamma(\omega_0^2 + \gamma^2)} \right\} \alpha(\omega) \tag{2.8}$$

At this point, it should be noted that as long as $\Delta\omega << \omega_0$, the evaluation of the integral in Eq. (2.6), depends primairly on the absorption and hence dispersion in the immediate vicinity of the resonance center [15]. The successful use of the Kramers-Kronig relations, depends, in their content, in the fact that negligible error results from a lack of knowledge of frequency spectrum remote from the point of interest (in our case, outside the vicinity of resonance frequency) [7]. To integrate Eq. (2.6) using the Lorentzian approximation, we use actual measured values for magnitude of peak absorption, $\alpha(\omega_0)$, peak frequency, ω_0, and the linewidth, 2γ. Since in the vicinity of resonance, the actual absorption line shape is almost Lorentzian, one is led to the conclusion that the use of a Lorentzian lineshape in Eq. (2.6) can be expected to give almost the same results as the numerical integration in the vicinity of resonance.

For the Lorentzian approximation, combining Eqs. (2.4) and (2.8) into Eq. (2.1) gives the final expression for reflectance for any absorbing medium in terms of basic information about its absorption coefficient. This expression is Eq. (2.1), repeated here for convenience:

$$\Re_p = \frac{a^2 + b^2 + Z^2 - 2|Z\{a\cos(\theta/2) + b\sin(\theta/2)\}|}{a^2 + b^2 + Z^2 + 2|Z\{a\cos(\theta/2) + b\sin(\theta/2)\}|} \tag{2.9}$$

where however, now

$$a = \left\{ n_1 + \left[\frac{c(\omega_o^2 - \omega\omega_o - \gamma^2)}{2\gamma(\omega_o^2 + \gamma^2)} \right] \alpha(\omega) \right\}^2 - \left\{ \frac{c^2}{4\omega^2} \alpha^2(\omega) \right\}$$

$$b = \left\{ n_1 + \left[\frac{c(\omega_o^2 - \omega\omega_o - \gamma^2)}{2\gamma(\omega_o^2 + \gamma^2)} \right] \alpha(\omega) \right\} \frac{c}{\omega} \alpha(\omega)$$

and Z and θ are as previously defined in terms of a, b and ϕ.

Predictions for reflectance using the actual absorption lineshape (numerical integration) and the Lorentzian approximation are compared with each other and with experimental measurements, in the following section.

2.4. EXPERIMENTAL

The solution of Rhodamine B in ethanol was selected as the lossy refractive medium from which reflections of collimated light beams are measured at the air medium interface. Rhodamine B was selected because it has a well defined absorption resonance in the green-yellow spectral region (Fig.2.1) which is readily accessible to the cw organic dye laser used to provide the tunable collimated light beam. Furthermore, the absorption spectrum, in the vicinity of the resonance, is reasonably close to the Lorentzian shape assumed in Section 2 above to facilitate the evaluation and the numerical calculations needed to make theoretical predictions (see comparison in Fig. 2.1). Actually measured values for magnitude of peak absorption, peak wavelength, and the linewidth, were those used in the Lorentzian approximation to evaluate theoretical expressions.

The actual experimental set up is relatively straight forward. A polarized collimated light beam is obtained from a tunable cw dye laser. By appropriate geometric arrangements of mirrors, the angle of incidence of the laser beam on the dye solution surface can be varied, and the incident and reflected powers at the dye-air interface measured using pv detectors. To increase sensitivity and accuracy, a phase locked loop amplifier was used in conjunction with the detectors. Measurements and comparisons with theoretical predictions were made for the "p" polarized ray only, since results

for the "s" polarization are expected to differ only in some details, that would not be expected to add to the understanding of the process or the confirmation of the models used.

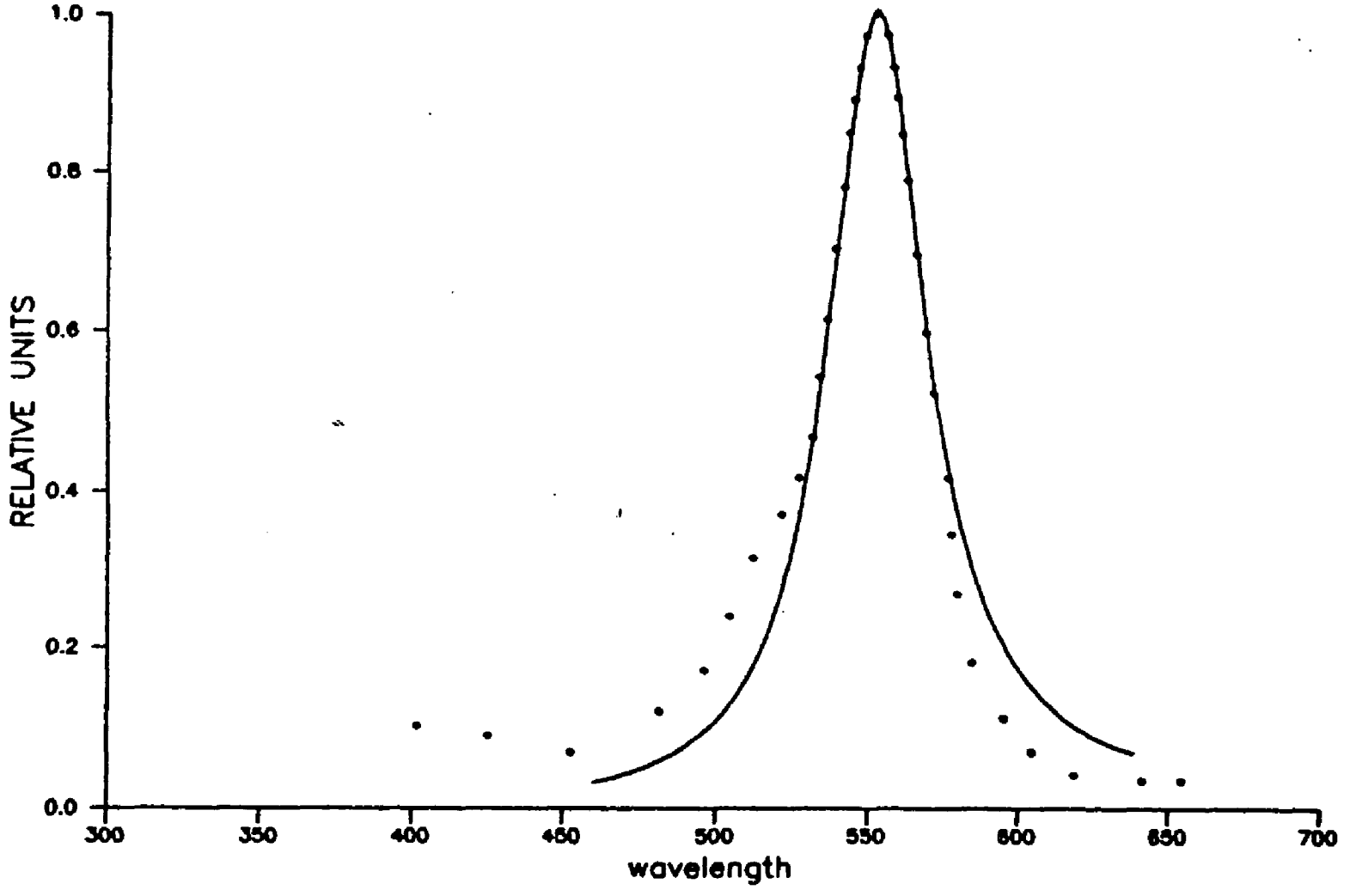

Fig 2.1 Absorption spectrum of Rhodamine B in Ethanol
—— Lorentzian • • • experimental

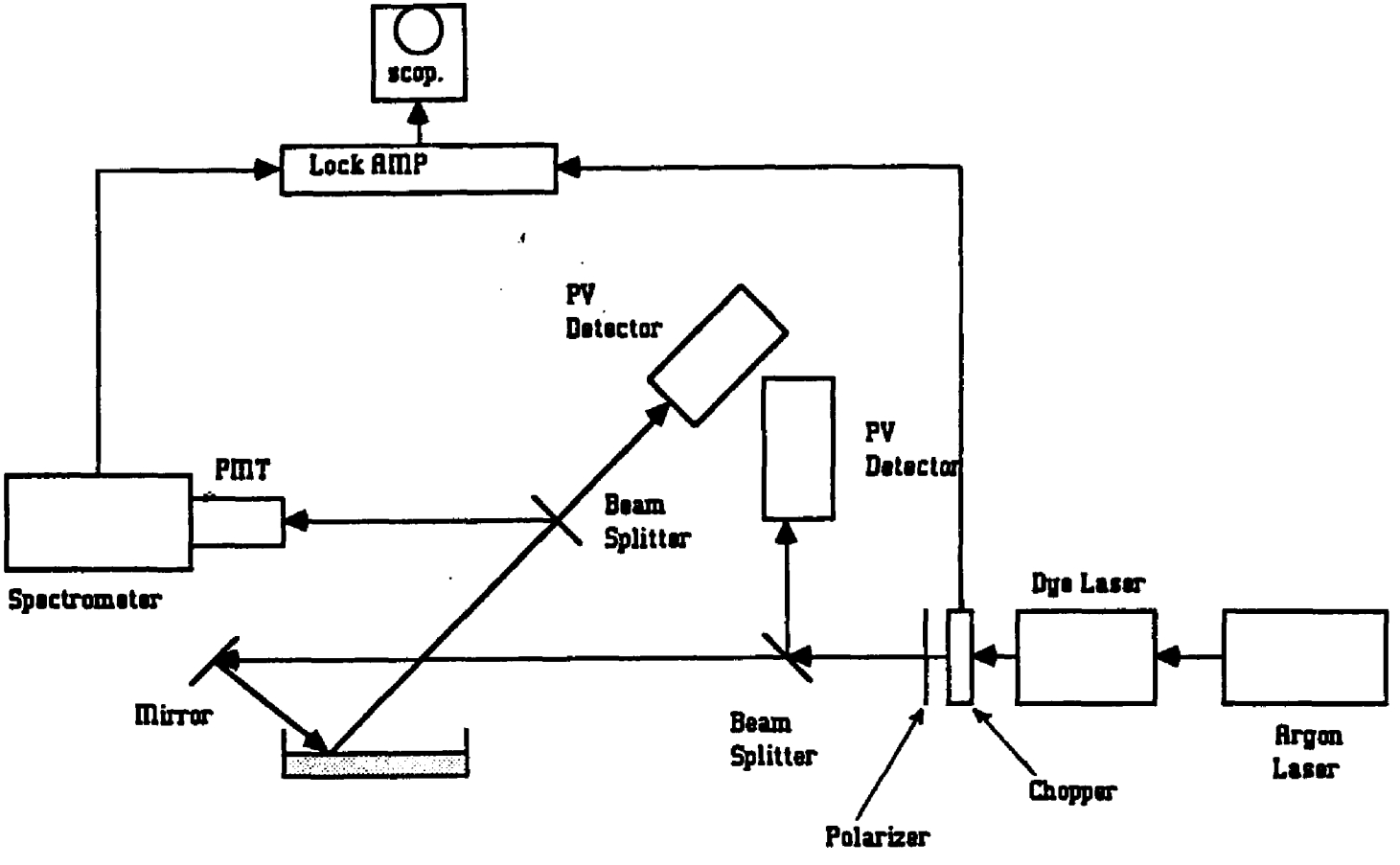

Fig 2.2 Experimental Setup for Reflection Measurements

2.5. COMPARISONS OF THEORETICAL PREDICTIONS AND EXPERIMENTAL RESULTS

The following parameters were measured experimentally and used in theoretical calculations:

i) an absorption peak (λ_o) at 552 nm,

ii) a line width ($\Delta\lambda$) of approximately 40 nm,

iii) a peak absorption coefficient, α (ω_o) of 5×10^4 cm^{-1}.

The arbitrary constant (n_1) in Eq. (2.10) is assigned a value of 1.364, which is the refractive index of the solvent (ethanol) used in our experiment. This is understood by assuming a zero value to the absorption coefficient (α) in Eq. (2.10), thus the medium is now lossless and its refractive index is reduced to the refractive index of the transparent solvent.

Experimental results and their theoretical comparisons are divided into three different sets.

SET I

Experimental measurements were carried out to determine and measure the reflectance as a function of wavelength at three different angles, 29°, 54°, and 75° respectively. As will be seen later, the significance of choosing the angle 54° is that this is the angle of minimum reflection, or Pseudo-Brewster angle (PB), at the resonance frequency. It is also close to the theoretically calculated and experimentally measured value of Brewster's angle for the ethanol solvent alone.

Figs. 2.2, 2.3, and 2.4 show the experimental results along with theoretical predictions. The theoretical predictions are made:
(i) using the Lorentzian approximation evaluated with actual measured values for magnitude of peak absorption, peak wavelength, and the linewidth, and
(ii) by carring out numerical integrations using the actual absorption line shape.

The theoretical predictions are carried out and compared with each other and with the experimental results of this set in Figs. 2.2, 2.3, and 2.4. These comparisons show a good agreement between the Lorentzian approximation and the numerical integration using the actual absorption line shape. Off resonance, where the difference between the Lorentzian line shape and the actual line shape is clear, α has a small value, and R_p values are in general less sensitive to variations in α. In order to more readily appreciate the relationship between the absorption and the reflectance curves, the theoretically assumed (Lorentzian) absorption spectrum is also shown, with, however, the same peak and linewidth as are measured experimentally.

When the angle of incidence is 29^o, the maxima for the reflectance is shifted towards longer wavelengths, when it is 75^o the maxima for the reflectance is shifted towards shorter wavelengths, while there is no shift at all when the angle of incidence is 54^o (PB angle at resonance). It is also interesting that the closest fit

between theoretical predictions and experimental results is obtained when the angle of incidence is the PB angle at resonance.

With the reasonableness of the Lorentzian approximation thus established, the remaining figures show only theoretical predictions based on the Lorentzian approximation, along with results of experimental measurements.

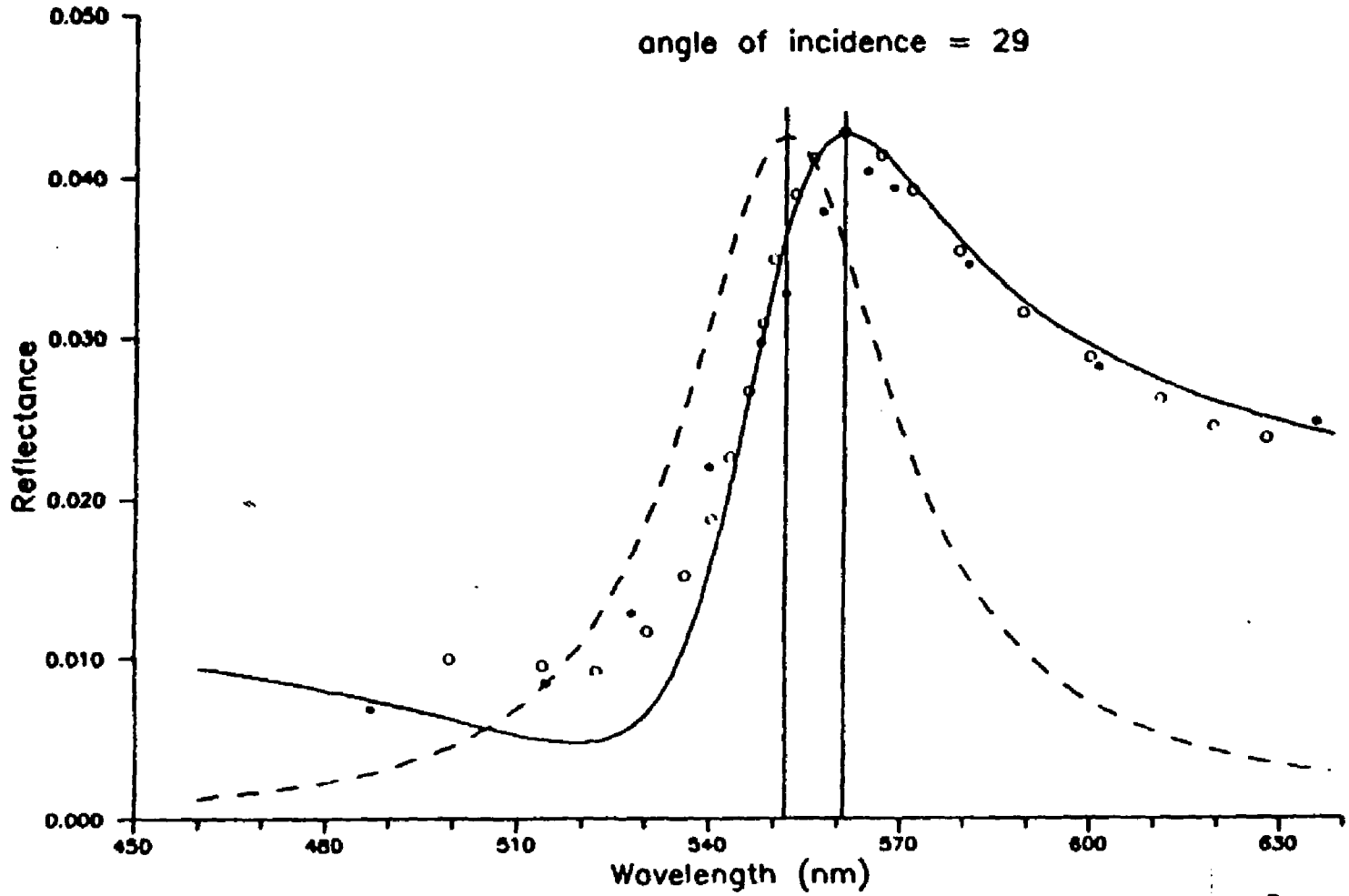

Fig 2.3 Reflectance R_p vs. λ for Rh B solution at angle of incidence $\phi = 29^o$

——— theoretical (Lorentzian) theoretical (actual lineshape)

• • • experimental - - - absorption spectrum

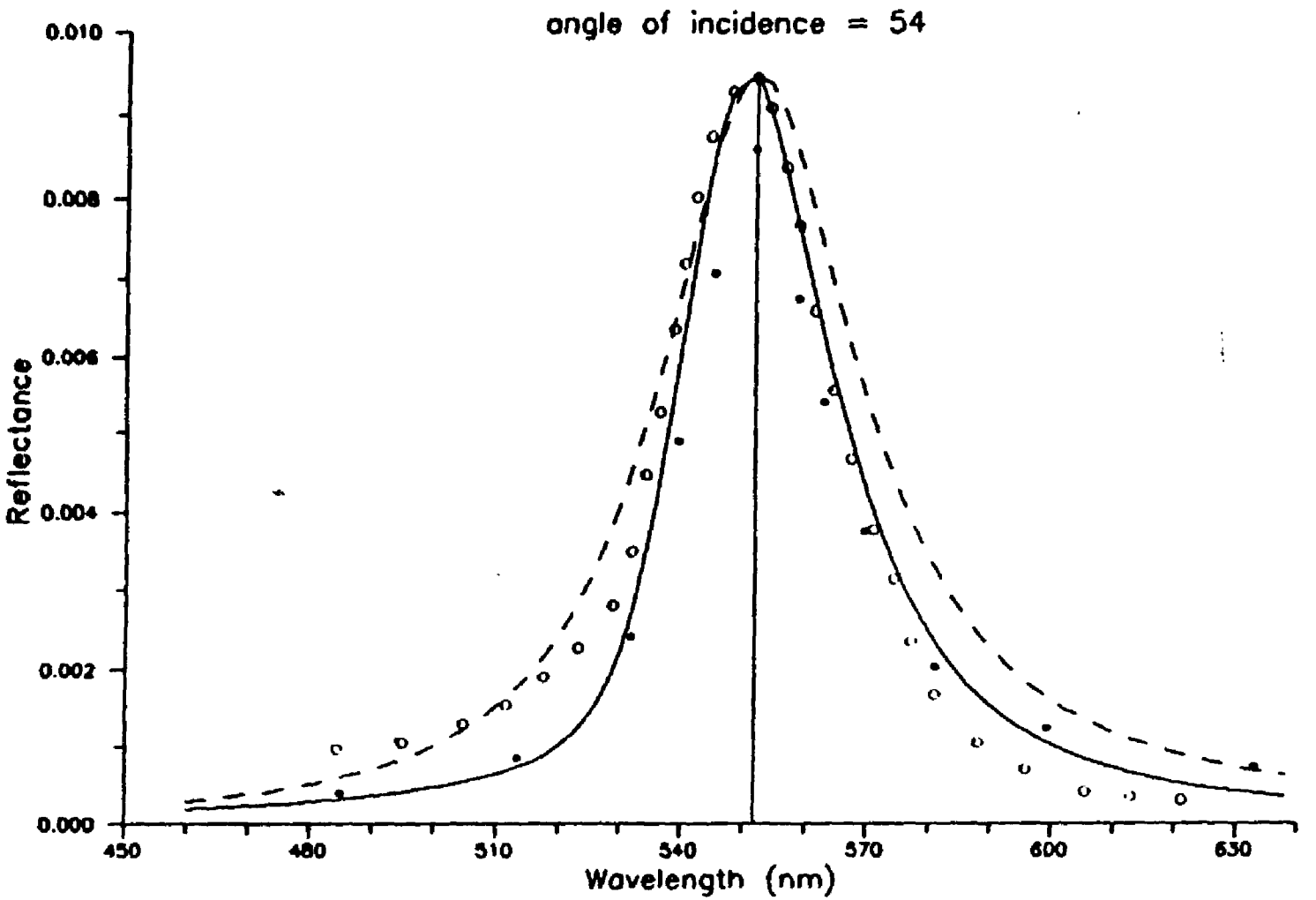

Fig 2.4 Reflectance R_p vs. λ for Rh B solution at angle of incidence $\phi = 54^o$

—— theoretical (Lorentzian) o o o theoretical (actual lineshape)

• • • experimental - - - absorption spectrum

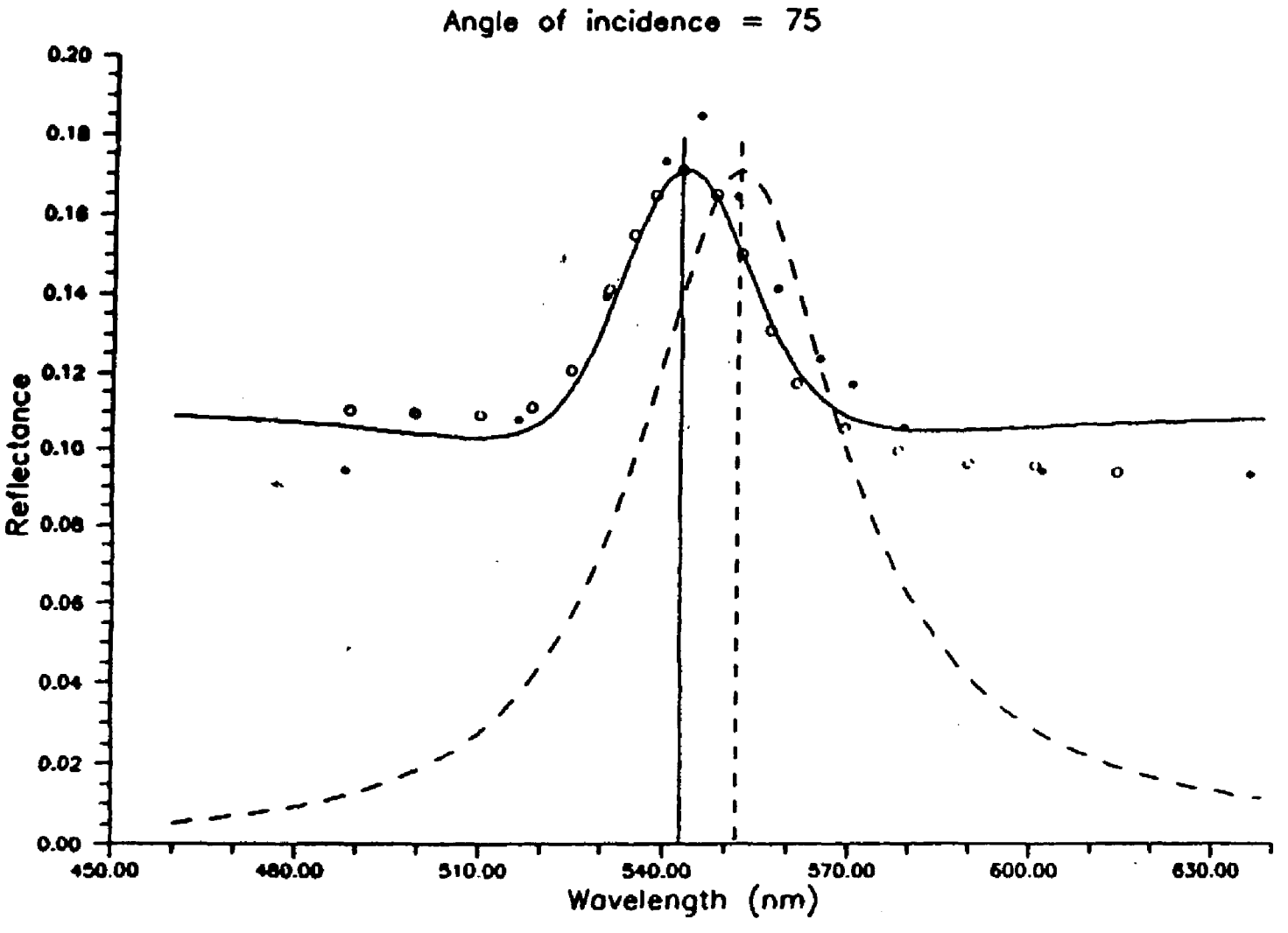

Fig 2.5 Reflectance Rp vs. λ for Rh B solution at angle of incidence ϕ = 75o

—— theoretical (Lorentzian) o o o theoretical (actual lineshape)

• • • experimental - - - absorption spectrum

SET II

Theoretical predictions using the Lorentzian approximation and experimental measurements were carried out to predict and measure the reflectance as a function of the angle of incidence for three different wavelengths, 514 nm, 552 nm, and 580 nm respectively. Figs. 2.5 and 2.6 show the theoretical predictions and the corresponding experimental measurements for the reflectance (R_p) vs. the angle of incidence (ϕ) at these wavelengths respectively. It is seen that there is no angle which corresponds to exactly zero reflection. The angle at which R_p has a minimum value is called the Pseudo-Brewster (PB) angle.

From Fig. 2.5 (theoretical result), we have:
at λ= 514 nm, ϕ_{pB}(incident angle of minimum reflectance) = 50^o, and the corresponding reflectance Rp = 0.0005. At λ= 552 nm, ϕ_{pB} = 53.7^o, and Rp = 0.01. At λ = 580 nm, ϕ_{pB} = 57.5^o, and Rp = 0.001.

Again, there is reasonably good agreement between theoretical predictions and experimental results Fig. 2.6 particularly at the resonance wavelength (552 nm). Fig. 2.5 is redrawn in Fig. 2.7, with a different scale, to more readily distinguish between the data.

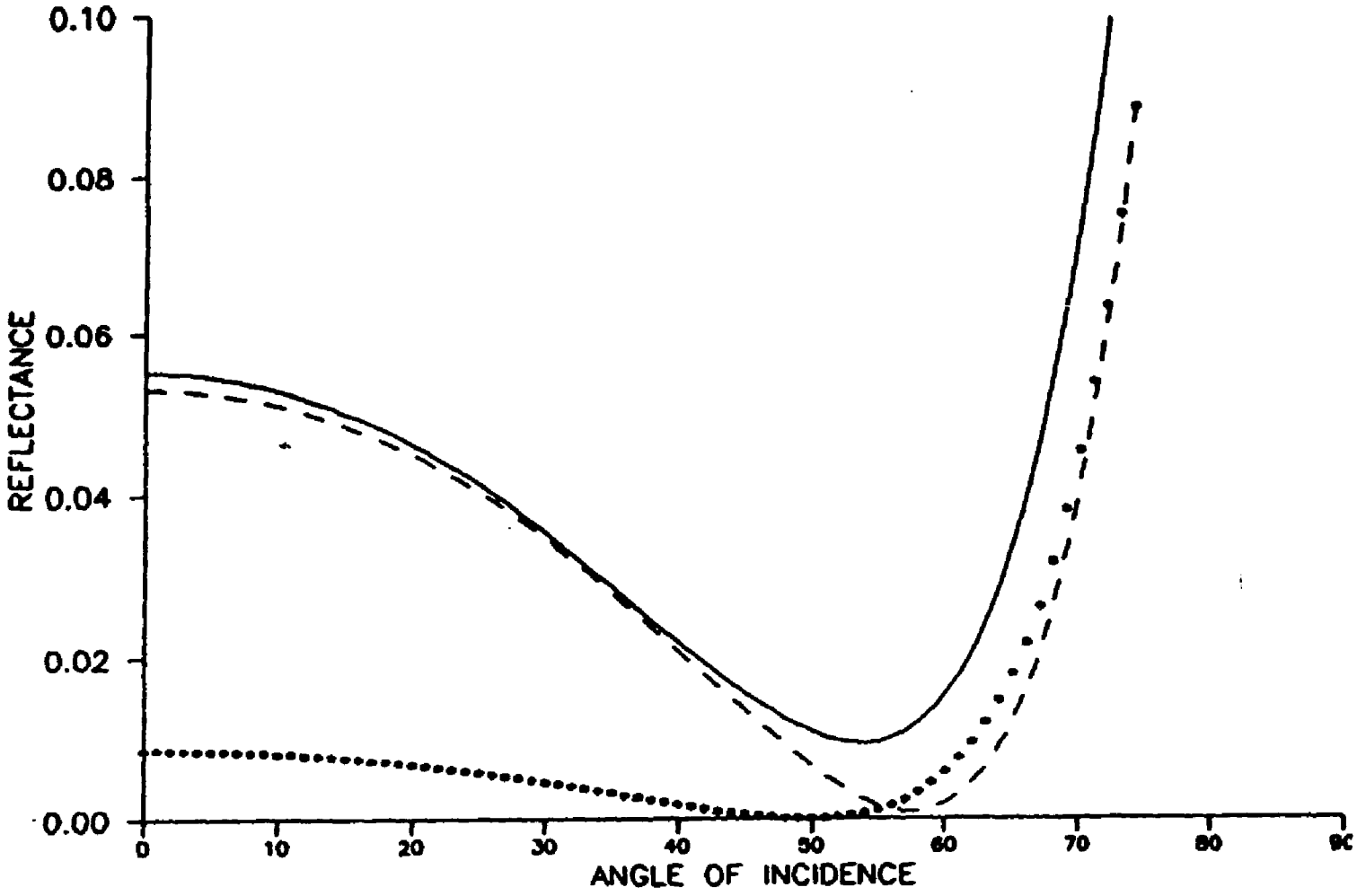

Fig. 2.6 Theoretical predictions of reflectance Rp vs. angle of incidence ϕ at wavelengths λ = 514, 552, and 580 nm
___ 552 nm, - - - 580 nm, • • • 514 nm

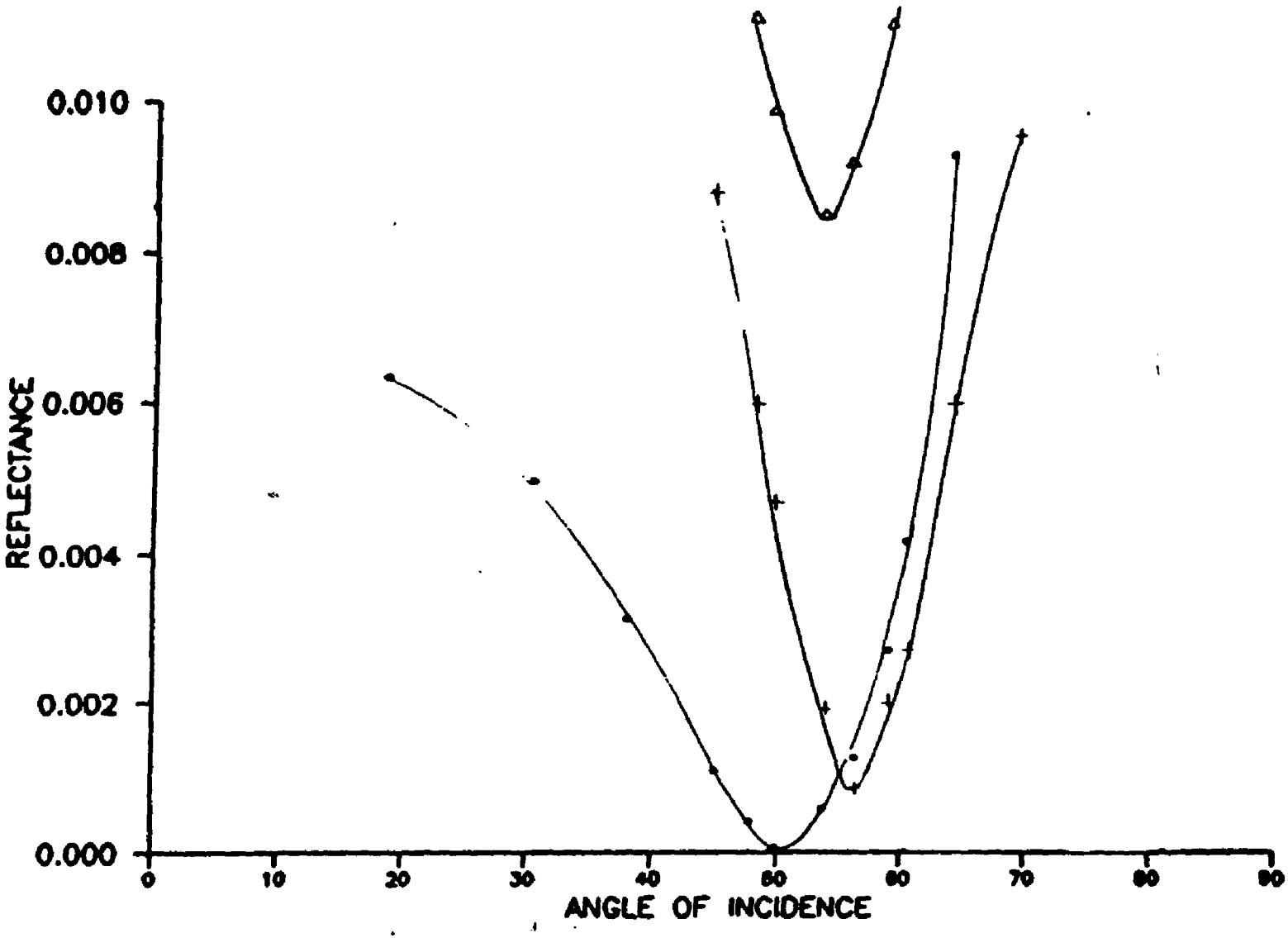

Fig.2.7 Experimental measurements of reflectance Rp vs. angle of incidence ϕ at wavelengths λ= 514, 552,and 580 nm ,
Δ Δ Δ 552 nm, + + + 580 nm , . . . 514 nm

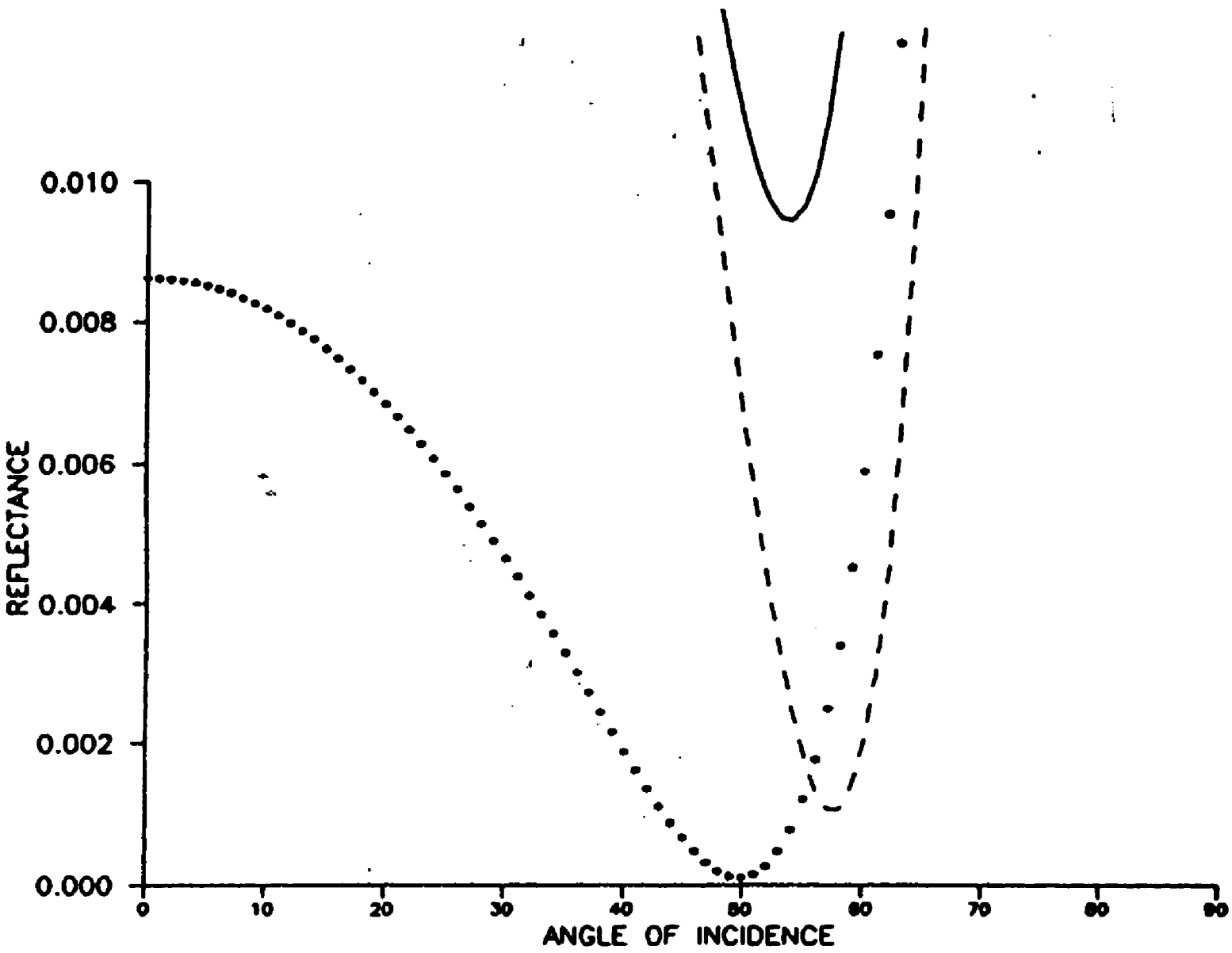

Fig. 2.8 Expansion of Fig.5 with the scale used in Fig. 6 to more readily distinguish between the data

SET III

Theoretical predictions again using the Lorentzian approximation and experimental measurements were carried out to predict and measure the Pseudo- Brewster angles and the reflectance corresponding to these angles vs. λ. It would be emphasized that, for any given λ, the PB angles were not determined by setting R_p in Eq. 2.3 equal to zero and then finding the corresponding angle, since such a solution does not exist. Instead, for a given λ, R_p was calculated for all ϕ's from $\phi = 0 - 90^{o}$, with increments of 0.01^{o}, and the angle with corresponding to the minimum reflectance is considered as the PB angle for that λ.

Fig. 2.8 shows the theoretical predictions and the experimental measurements for ϕ_{pB} vs. λ. Fig. 2.9 shows the theoretical predictions and the experimental measurements for reflectance at the PB angles vs. λ, showing a good fit between experimental and theoretical results and with the reflectance at the PB angles tracking the absorption.

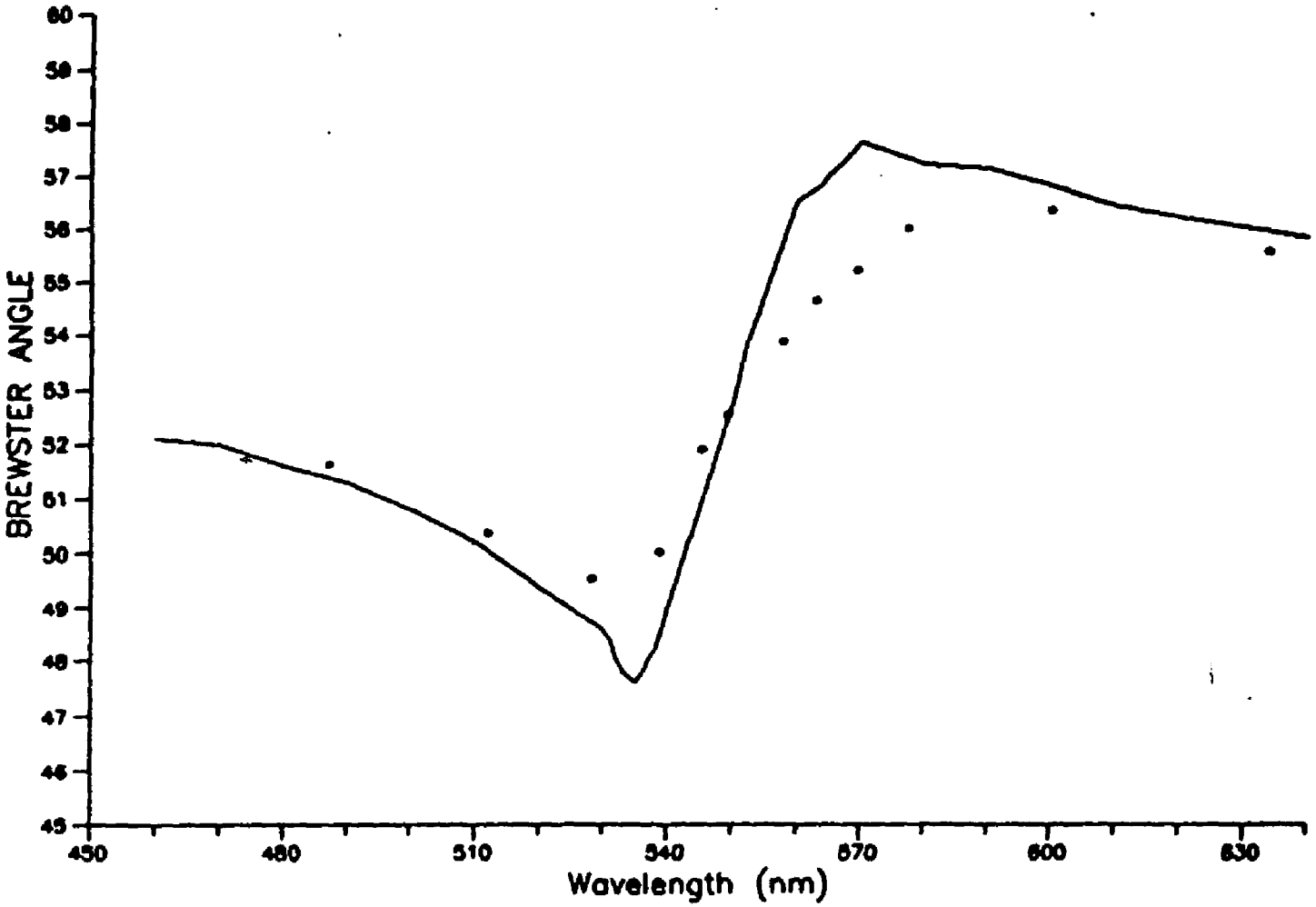

Fig. 2.9 Pseudo-Brewster angle ϕ_{pB} vs. λ

——— theoretical

• • • experimental

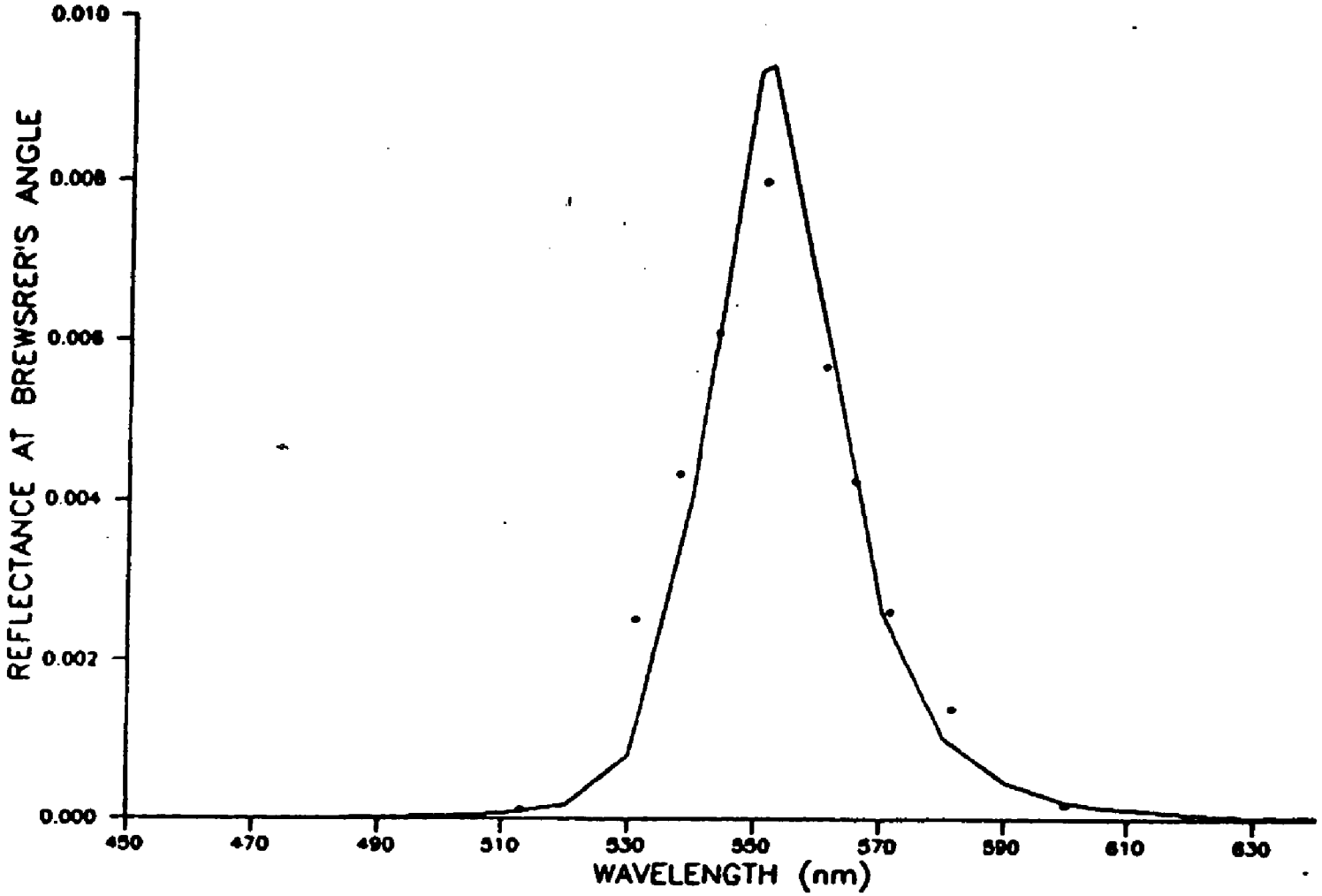

Fig. 2.10 **Reflectance at Pseudo-Brewster angles vs. λ**

_____ **theoretical**

. . . . **experimental**

2.6. CONCLUSION

We have reported experimental work on surface reflections measurements at the planar interface of resonantly absorbing medium and the air for a variety of situations. An ethanolic solution of Rhodamine B, an organic laser dye luminofor with a well defined resonance absorption spectrum, was used as the absorbing medium. It was found that the maxima for reflectance coincide with the maxima for absorption when the angle of incidence is equal to the PB angle at resonance frequency. However, the maxima might be shifted to longer or shorter wavelengths depending on the angle of incidence. It was also found that the PB angle at resonance frequency is equal to the Brewster's angle for the solvent (lossless medium).

The Fresnel reflectivity equations combined with the Kramers-Kronig relations were used to predict the reflectance in terms of the known absorption coefficient. Our experimental results generally confirm the theoretical predictions.

CHAPTER 3
On the State of Polarization of a Reflected Beam from a Resonantly Absorbing Medium

3.1.BASIC PARAMETERS OF POLARIZATION:

3.1.1.Introduction:

There are many reasons why problems of polarization and depolarization deserve intimate study. In many cases observation of changes in polarization permits deeper insight into physical phenomena. In addition, the solutions of polarization and depolarization problems have a host of practical applications, some of which come under one of the following three groups:

Optimization. In many cases, a certain type of polarization will accomplish a given task better than another.

Discrimination. Unwanted reflections and other causes, often lead to the presence of two signals of which only one is wanted and the other interferes, yet separation by frequency, amplitude or phase proves difficult or impossible. Often the two signals, differ, or can be made to differ in polarization, and this can be used to discreminate against one of them.

Identification. Since different of scatterers and propagation media will produce different types and degrees of depolarization, it is often possible it infer what type of scatterers, what type of medium, what

type of geometrical configuration of scatterers, etc., must have been responsible for an observed type of depolarization.

Since the work reported here utilizes polarization and depolarization, some study of polarization and depolarization is necessary. In this chapter the various parameters related to polarization and depolarization that may have an impact on the depolarization of the reflected beam are discussed.

3.2 Properties of polarized light:

3.2.1 Basic definitions-linear Polarization:

An electromagnetic wave propagating in the direction of the unit vector k has four basic characteristics: amplitude, phase, frequency and polarization.

The term ***polarization*** is used to describe the statistical fluctuations of the direction of the electric vector E of the electromagnetic wave. Figure 3.2.1 shows the orientaion of the electric vector E at an instant of time for an electromagnetic wave. The plane defined by E and the propagation vector k at a point is called the ***polarization plane***. The orientation of the electric field E, with respect to a reference plane, at a given point in space, during one period of oscillation is called the ***direction of polarization.*** The angle between the polarization plane and the reference plane at a point is called the ***polarization angle***. As a reference plane is usually taken the horizontal plane if the surface of the earth is relevant or the plane of incidence (determined by the incident and reflected or scattered beam axes) in scattering problems.

An electromagnetic wave is linearly polarized if the polarization plane has constant orientation (constant polarization angle) at any point. Figure 3.2.2 shows a linearly polarized electromagnetic wave. The components of the electric vector E are expressed using two mutually perpendicular unit vectors in the plane perpendicular to k. These two unit vectors are oriented in privileged directions i.e. parallel and perpendicular to the reference plane. Depending on the application the parallel and perpendicular components of the electric vector E have different notations i.e. E^- and E^+, E_p and E_c, E_{11} and E_-, E_h and E_v, E_x and E_y respectively. Figure 3.2.1 shows the orientation of the electric vector E at an instant of time for an electromagnetic wave. Considering the horizontal plane as the reference plane, a linearly polarized wave with polarization plane parallel or perpendicular to the horizontal plane is called horizontally or vertically polarized respectively.

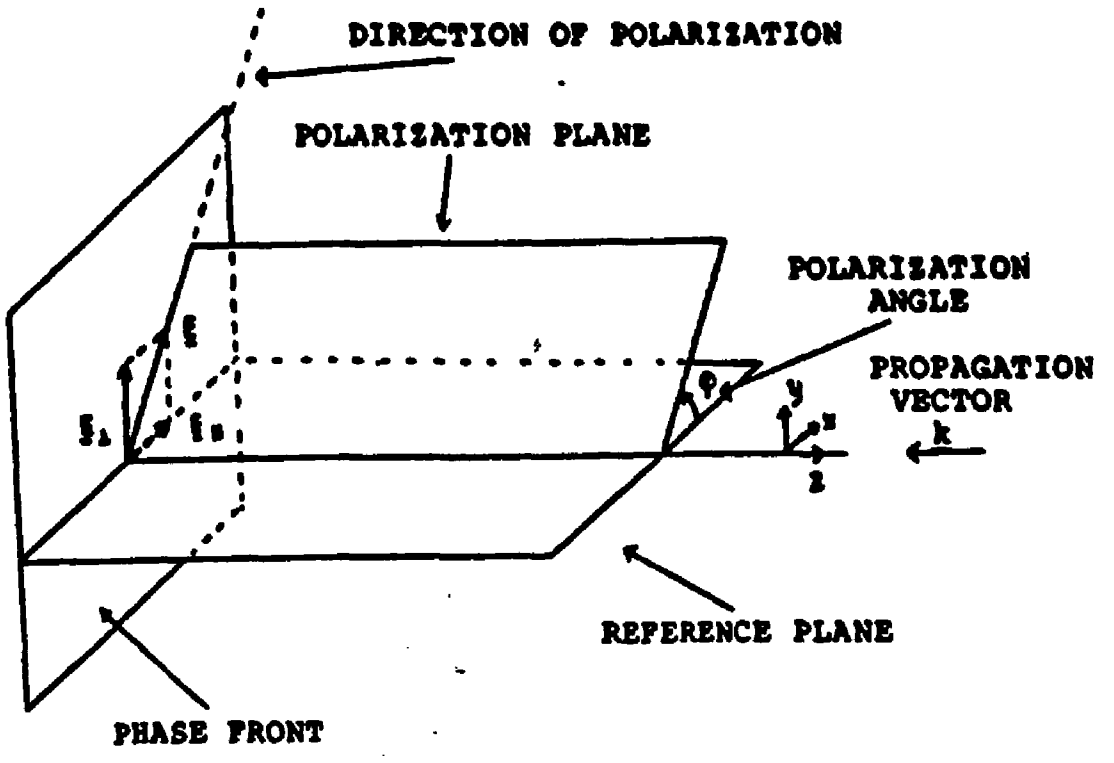

FIG. 3.2.1 Orientation of the electric vector E at an instant of time, with respect to the plane of reference for a wave propagation along the z direction.

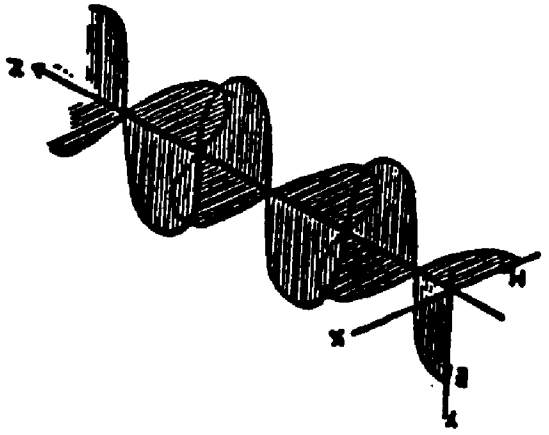

FIG. 3.2.2 Linearly polarized plane electromagnetic wave.

3.2.2 Elliptic Polarization:

For an electromagnetic wave propagated along the z-axis, with the E and H vectors vibrating harmonically in the xy plane, the two Cartesian components are given by

$$E_x = E_x \exp\{j(\tau + \Delta_x)\}$$
$$E_y = E_y \exp\{j(\tau + \Delta_y)\} \qquad (3.2.1)$$

where $\tau = (wt - kz)$

Considering the real parts for E_x, E_y and eliminating τ, the locus of E can be eliminated from the resulting equation

$$\left(\frac{E_x}{E_{x_o}}\right)^2 + \left(\frac{E_y}{E_{y_o}}\right)^2 - 2\left(\frac{E_x E_y}{E_{x_o} E_{y_o}}\right)\cos\Delta = \sin\Delta \qquad (3.2.2)$$

where $\Delta = \Delta_x - \Delta_y$

Which is the equation of an ellipse and is depicted in Figure(3.2.3). The value of Δ determines the form of the elliptical vibration as shown in Figure (3.2.4) . This ellipse represents a projection on the xy plane of locus of the magnitude of the extreme values of the

electric vector (the amplitude), and for this general case the wave is said to be elliptically polarized.

The sides of the rectangle in which the ellipse is inscibed are parallel to the coordinate axes and have lengths $2E_{xo}$ and E_{yo}. The ellipse touches the sides at the points ($\pm E_{xo}, \pm E_{yo} \cos \Delta$) and ($\pm E_{xo} \cos \Delta, \pm E_{yo}$). The major axis of the ellipse is inclined at an angle Ψ with respect to the x-axis given by

$$\tan 2\Psi = \left(\frac{2E_{xo}E_{yo}}{E^2_{xo} - E^2_{yo}} \right) \cos \Delta , \qquad 0 \leq \Psi \geq \Pi \tag{3.2.3}$$

The major and minor axes of the ellipse, A and B respectively, are given by

$$A^2 = E^2_{xo} \cos^2 \quad + E^2_{yo} \sin^2 \quad + 2E_{xo} E_{yo} \cos \sin \cos \Delta$$

$$B^2 = E^2_{xo} \cos^2 \quad + E^2_{yo} \sin^2 \quad - 2E_{xo} E_{yo} \cos \sin \cos \Delta \tag{3.2.4}$$

Defining

$$\frac{E_{yo}}{E_{xo}} = \tan \alpha, \qquad (0 \leq \alpha \leq \tfrac{\pi}{2}) \tag{3.2.5}$$

and

$$\pm \tfrac{B}{A} = \tan \gamma, \qquad (-\pi / 4 \leq \gamma \leq \pi / 4) \tag{3.2.6}$$

where the ratio B/A is called the ellipticity, the following usefull relationships are valid

$$\tan 2\Psi = (\tan 2\alpha)\cos\Delta \qquad (3.2.7)$$

$$\sin 2\gamma = (\sin 2\alpha)\sin\Delta \qquad (3.2.8)$$

$$\cos 2\alpha = +(\cos 2\gamma)\cos 2\Psi \qquad (3.2.9)$$

In addition conservation of light intensity (Energy) gives

$$E^2_{xo} + E^2_{yo} = A^2 + B^2 \qquad (3.2.10)$$

Also if Z_o is the intrinsic impedence for plane waves the intensity is given by

$$I = (A^2 + B^2)/2Z_o \qquad (3.2.11)$$

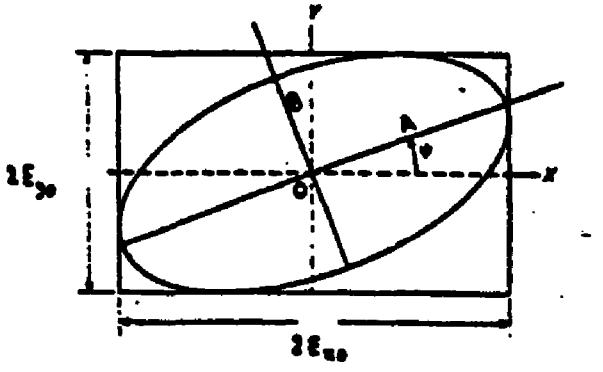

FIG. 3.2.3 Vibration ellipse for the electric vector.

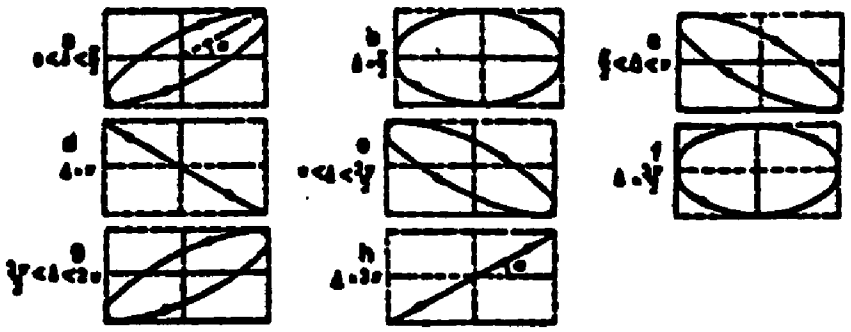

FIG. 3.2.4 Vaibration in the form of an elliptical vibration with phase difference.

3.2.3 Polarization and Depolarization Factors:

For A plane electromagnetic wave with propagation vector k the electric field E as vector-phasor can be resolved in two components Horizontal and Vertical

$$E = E_x e_x + E_y e_y \qquad (3.2.12)$$

where e_x and e_y are the corresponding unit vectors.
Considering E_x and E_y as complex phasors, for monochromatic wave with frequency ω, the complex polarization factor is defined as

$$p = E_y / E_x \qquad (3.2.13)$$

The polarization factor is in general a complex quantity.

$$p = |p| \exp\{j\arg(p)\} = (E_y/E_x) \exp\{j\arg(E_y) - j\arg(E_x)\}$$

$$= (E_{yo}/E_{xo}) \exp\{j\Delta\} \qquad (3.2.14)$$

where

$$|p| = E_{yo}/E_{xo} \qquad (3.2.15a)$$

and

$$\arg(p) = \Delta \qquad (3.2.15b)$$

are the ratio of the amplitudes and the phase defference respectively between the two components of the wave.

Since any elliptic polarization can be produced by superposition of two mutually perpendicular polarizations, with the corresponding amplitude and phase shift, it follows that the complex polarization factor describes the polarization of an electromagnetic wave uniquely. It is shown in Equations 3.2.15 that the parameters of the polarization ellipse, involved in equations 3.2.1 through 3.2.11, can be obtained from p.

Another important quantity for polarization defined as

$$p = I_p / (I_p + I_u) \qquad (3.2.16)$$

where I_p is the intensity of the polarized component and I_u is the intensity of the unpolarized component.

A change in polarization suffered by an electromagnetic wave as consequence of propagation, reflection, scattering, diffraction or any other interaction with matter, is called depolarization. For an incident linearly polarized field E_1 subjected to electromagnetic process causing depolarization, the resulting field E_2 can be expressed as

$$E_2 = E_{2p} + E_{2c} \qquad (3.2.17)$$

where E_{2p} is the component parallel to the incident field E_1 and E_{2c} is the cross-polarized component, perpendicular to the incident field

E_1. If I_2 and p_2 are the intensity and power respectively corresponding to E_2, the linear depolarization ratio δ is defined as

$$\delta = E_c/E_p = p_c/p_p = I_c/ I_p \qquad (3.2.18)$$

In case of depolarization due to backscattering, using β_c and β_p, the backscattering coefficients of the two components of E_2, δ can be expressed as

$$\delta = \beta_c/\beta_p \qquad (3.2.19)$$

Depending on the interaction, E_c may be completely unpolarized or polarized with phase difference with respect to E_p, resulting in elliptically polarized field E_2. In the second case the depolarization ratio can be expressed in terms of the parameters of the polarization ellipse. In general, after an intgration, the orientation of the major semiaxis of the polarization ellipse with respect to the reference plane is different from the orientation of the incident field E_1. If the orientation difference is an angle ψ, the depolarization ratio δ can be expressed as

$$\delta = (B^2 + A^2 \tan^2 \psi)/(B^2 \tan^2 \psi + A^2) \qquad (3.2.20)$$

3.3. The State of Polarization:

3.3.1: Introduction:

Experiments on the reflection of polarized monochromatic laser light at the planar interface of resonantly absorbing medium and the air, to measure its state of polarization after reflection, were made for a variety of situations, including Brewster's angle in the spectral vicinity of the resonance wavelength. An ethanolic solution of Rhodamine B, an organic laser dye luminofor with a well defined resonance absorption spectrum, was chosen as the absorbing medium. The tunable polarized output of a cw dye laser is used to provide the collimated monochromatic beam. To compare the experimental results with theory, the Fresnel reflectivity equations combined with the Kramers-Kronig relations were used to derive expressions to predict the state of polarization of the reflected beam in terms of the known absorption coefficient. The experimental results generally confirm the theoretical predictions.

3.4. THEORY

3.4.1 GENERAL

In this section we develop the analytical expressions required to predict the fractional depolarization, D, for the reflectance of a monochromatic collimated light beam at the planar interface between a transparent medium of incidence (usually air, $\varepsilon_0 = 1$) and an absorbing medium of refraction (ε_1 complex). These expressions are derived in terms of the absorption coefficient (α) of the medium (assuming it is known or can be measured), the angle of incidence, and the wavelength of the incident beam.

To obtain the expressions for fractional depolarization of the reflected light, in the desired form, the Fresnel coefficient for the P-polarized beam (r_P) has been put into the form: $r_P = A + j\psi$ (where A and Ψ are written in terms of these three parameters and the real part (n) of the complex refractive index of the absorbing medium). Then, using the Kramers-Kronig relationships, an analytical expression for the real part of the complex refractive index is obtained in terms of the absorption coefficient (i.e. the imaginary part of the complex refractive index of the absorbing medium). This result is then combined with the Fresnel coefficient (r_P) to predict the fractional depolarization of the reflected beam, D, at any given wavelength, solely in terms of the absorption coefficient of the medium at that wavelength and the angle of incidence.

The fractional depolarization of the reflected beam, D, is defined as:

$D = \sin \mu$, where μ is the angle between the planes of polarization of the incident P- polarized beam and the reflected beam. Equivalently D can be defined as:

$$D^2 = \Psi^2 / R_p$$

where, $R_p = r_p r_p^*$ is the power reflectance. These expressions were also used to predict the PB angles over the range of wavelengths of interest.

3.4.2 r_p IN THE FORM A+ JΨ

The reflection of a collimated light beam is governed by the Fresnel coefficients [10] , see appendix A

$$r_p = A + j\Psi \qquad (3.4.1)$$

The intensity (or power) reflectance R_p, is given by:

$$\Re_p = r_p \dot{r}_p$$

using Eq. (A.8) we get:

$$\Re_p = \left\{ \frac{\Omega_1\Omega_2 + \beta_1\beta_2}{\Omega_2^2 + \beta_2^2} \right\}^2 + \left\{ \frac{\beta_1\Omega_2 - \beta_2\Omega_1}{\Omega_2^2 + \beta_2^2} \right\}^2$$

$$= \frac{\Omega_1^2 + \beta_1^2}{\Omega_2^2 + \beta_2^2} \qquad (3.4.2)$$

substituting Eq. (A.6) into Eq. (3.4.1) gives:

$$\Re_p = \frac{a^2 + b^2 + Z^2 - 2|Z\{a\cos(\theta/2) + b\sin(\theta/2)\}|}{a^2 + b^2 + Z^2 + 2|Z\{a\cos(\theta/2) + b\sin(\theta/2)\}|} \qquad (3.4.3)$$

We next relate the real and imaginary quantities, a and b, to the absorption coefficient of the medium. The complex refractive index , N, is defined by: N = n + jk, where the imaginary part, k, is related to the absorption coefficient, α by:

$$k = \frac{c}{2\omega}\alpha(\omega) \qquad (3.4.4)$$

where c is the speed of light in free space and ω is the angular frequency.

The complex refractive index, N, is also related to the dielectric constant of the medium by the relation:

$$N^2 = \varepsilon = \{n^2 - k^2\} + j2nk = a + jb \qquad (3.4.5)$$

combining Eqs. (A.2), (3.4.4) and (3.4.5) gives:

$$a = n^2 - \frac{c^2}{4\omega^2}\alpha^2(\omega) \qquad b = n\frac{c}{\omega}\alpha(\omega) \tag{3.4.6}$$

This means that all the terms in Eq (3.4.2) are now available in terms of n and α (as well as ω, c, and ϕ).

3.5. REFLECTANCE IN TERMS OF α

We now turn to the second part of the problem to find $n(\omega)$ in terms of the absorption coefficient $\{\alpha(\omega)\}$, so that the solution of Eq.(3.4.2) can be obtained in terms of the absorption coefficient only.

Since the imaginary part $\{k(\omega)\}$ of the complex refractive index is given by Eq. (3.4.4) in terms of α and ω, using the Kramers-Kronig relations, the real part $\{n(\omega)\}$ can also be determined in terms of α and ω within an arbitrary constant (n_1) which can be calculated from the specific physical conditions. The Kramers-Kronig relation for the real part $n(\omega)$ is given by [3]:

$$n(\omega') = n_1 + \frac{1}{\pi}P.V.\int_{-\infty}^{\infty}\frac{k(\omega)}{(\omega - \omega')}d\omega \tag{3.5.1}$$

where P.V. means the Cauchy principal value.

It is important to stress the generality of the relation of Eq. (3.5.1). It requires only boundedness and causality [15]. These conditions are really no assumptions at all, for they are necessarily fulfilled by

virtue of the fact that the polarization of a wave cannot antecede the arrival of the disturbing electric field that produces it [6].
Rewriting Eq. (3.5.1) in terms of α (Eq.3.4.4) gives:

$$n(\omega') = n_1 + \frac{c}{2\pi} P.V. \int_{-\infty}^{\infty} \frac{\alpha(\omega)}{\omega(\omega - \omega')} d\omega \qquad (3.5.2)$$

To obtain reflectance in the vicinity of the absorption resonance, using Eq. (3.4.3), it is first necessary to evaluate the integration of Eq. (3.5.2) over the spectral range of interest, and then substitute the results into Eq. (3.4.3). To evaluate the integration in Eq. (3.5.2), two posibble approaches could be used. The first would be to carry out a numerical integration using the actual measured absorption line shape (Fig. 3.5.1).

The second approach is to assume a Lorentzian approximation for the absorption lineshape in the vicinity of the peak, and to analytically integrate Eq. (3.5.2) to get an analytical expression for $n(\omega)$. For this approach, we assume a Lorentzian function for the absorption coefficient $\alpha(\omega)$, given by:

$$\alpha(\omega) = \frac{\alpha(\omega_0)\gamma^2}{(\omega - \omega_0)^2 + \gamma^2} \qquad (3.5.3)$$

where:

$\gamma = (\Delta\omega / 2)$, and $\alpha(\omega_0)$ is the absorption coefficient at resonance Substituting Eq. (3.5.3) into Eq. (3.5.2) and carring out the integration we get (see appendix):

$$n(\omega) = n_1 + \left\{ \frac{c(\omega_0^2 - \omega\omega_0 - \gamma^2)}{2\gamma(\omega_0^2 + \gamma^2)} \right\} \alpha(\omega) \qquad (3.5.4)$$

At this point, it should be noted that as long as $\Delta\omega << \omega_0$, the evaluation of the integral in Eq. (3.5.2), depends primairly on the absorption and hence dispersion in the immediate vicinity of the resonance center [15]. The successful use of the Kramers-Kronig relations, depends, in their contest, in the fact that negligible error results from a lack of knowledge of frequency spectrum remote from the point of interest (in our case, outside the vicinity of resonance frquency) [7]. To integrate Eq. (3.5.2) using the Lorentzian approximation, we use actual measured values for magnitude of peak absorption, $\alpha(\omega_0)$, peak frequency, ω_0, and the linewidth, 2γ. Since in the vicinity of resonance, the actual absorption line shape is almost Lorentzian, one is led to the conclusion that the use of a Lorentzian lineshape in Eq. (3.5.2) can be expected to give almost the same results as the numerical integration in the vicinity of resonance.

For the Lorentzian approximation, combining Eqs. (3.4.5) and (3.5.4) into Eq. (3.4.3) gives the final expression for reflectance for

any absorbing medium in terms of basic information about its absorption coefficient. This expression is Eq. (3.4.3), repeated here for convenience:

$$\Re_p = \frac{a^2 + b^2 + Z^2 - 2|Z\{a\cos(\theta/2) + b\sin(\theta/2)\}|}{a^2 + b^2 + Z^2 + 2|Z\{a\cos(\theta/2) + b\sin(\theta/2)\}|} \tag{3.5.5}$$

where however, now

$$a = \left\{ n_1 + \left[\frac{c(\omega_0^2 - \omega\omega_0 - \gamma^2)}{2\gamma(\omega_0^2 + \gamma^2)} \right] \alpha(\omega) \right\}^2 - \left\{ \frac{c^2}{4\omega^2} \alpha^2(\omega) \right\}$$

$$b = \left\{ n_1 + \left[\frac{c(\omega_0^2 - \omega\omega_0 - \gamma^2)}{2\gamma(\omega_0^2 + \gamma^2)} \right] \alpha(\omega) \right\} \frac{c}{\omega} \alpha(\omega)$$

and Z and θ are as previously defined in terms of a, b and ϕ.

3.6 FRACTIONAL DEPOLARIZATION OF THE REFLECTED BEAM

Since the fractional of depolarization, D, of the reflected beam (assumed to be " P" polarized before reflection) is defined as:

$$D^2 = \Psi^2 / R_p \tag{3.6.1}$$

where Ψ is given from Eq. (3.4.8) by:

$$\psi = \frac{\beta_1\Omega_2 - \beta_2\Omega_1}{\Omega_2^2 + \beta_2^2} \tag{3.6.2}$$

substituting Eq. (A.6) into Eq. (3.6.2) gives:

$$\psi = \frac{2z\{b\cos(\theta/2) - a\sin(\theta/2)\}}{a^2 + b^2 + z^2 + 2|z\{a\cos(\theta/2) + b\sin(\theta/2)\}|} \tag{3.6.3}$$

Finally, combining Eqs. (3.4.3) and (3.6.2) into Eq. (3.6.3) gives the desired final expression for the fractional depolarization of the reflected beam, D, as:

$$D = \frac{4z^2\{b\cos(\theta/2) - a\sin(\theta/2)\}^2}{\{a^2 + b^2 + z^2\}^2 - \{2z[a\cos(\theta/2) + b\sin(\theta/2)]\}^2} \tag{3.6.4}$$

Predictions for fractional depolarization using the actual absorption line shape (numerical integration) and the Lorentzian approximation are compared with each other and with experimental measurements, in the following section.

3.7. EXPERIMENTAL

The solution of Rhodamine B in ethanol was selected as the lossy refractive medium from which reflections of collimated light beams were to be measured at the air medium interface. Rhodamine B was selected because it has a well defined absorption resonance in the green- yellow spectral region (Fig.2.1) which is readily accessible to the cw organic dye laser used to provide a tunable collimated light beam. Furthermore, the absorption spectrum, in the vicinity of the resonance, is reasonably close to the Lorentzian shape assumed in Section 2 above to facilitate the evaluation and the numerical calculations needed to make theoretical predictions in the vicinity of resonance (see comparison in Fig. 2.1). Actually measured values for magnitude of peak absorption, peak wavelength, and the linewidth, were those used in the Lorentzian approximation to evaluate theoretical expressions.

The actual experimental set up is straight forward. A polarized collimated light beam is obtained from a tunable cw dye laser. By appropriate geometric arrangements of mirrors, the angle of incidence of the laser beam on the dye solution surface can be varied, and the polarization of the reflected beam determined using rotating polarizers and pv detectors. To increase sensitivity and accuracy, a phase lock loop amplifier was used in conjunction with the detectors.

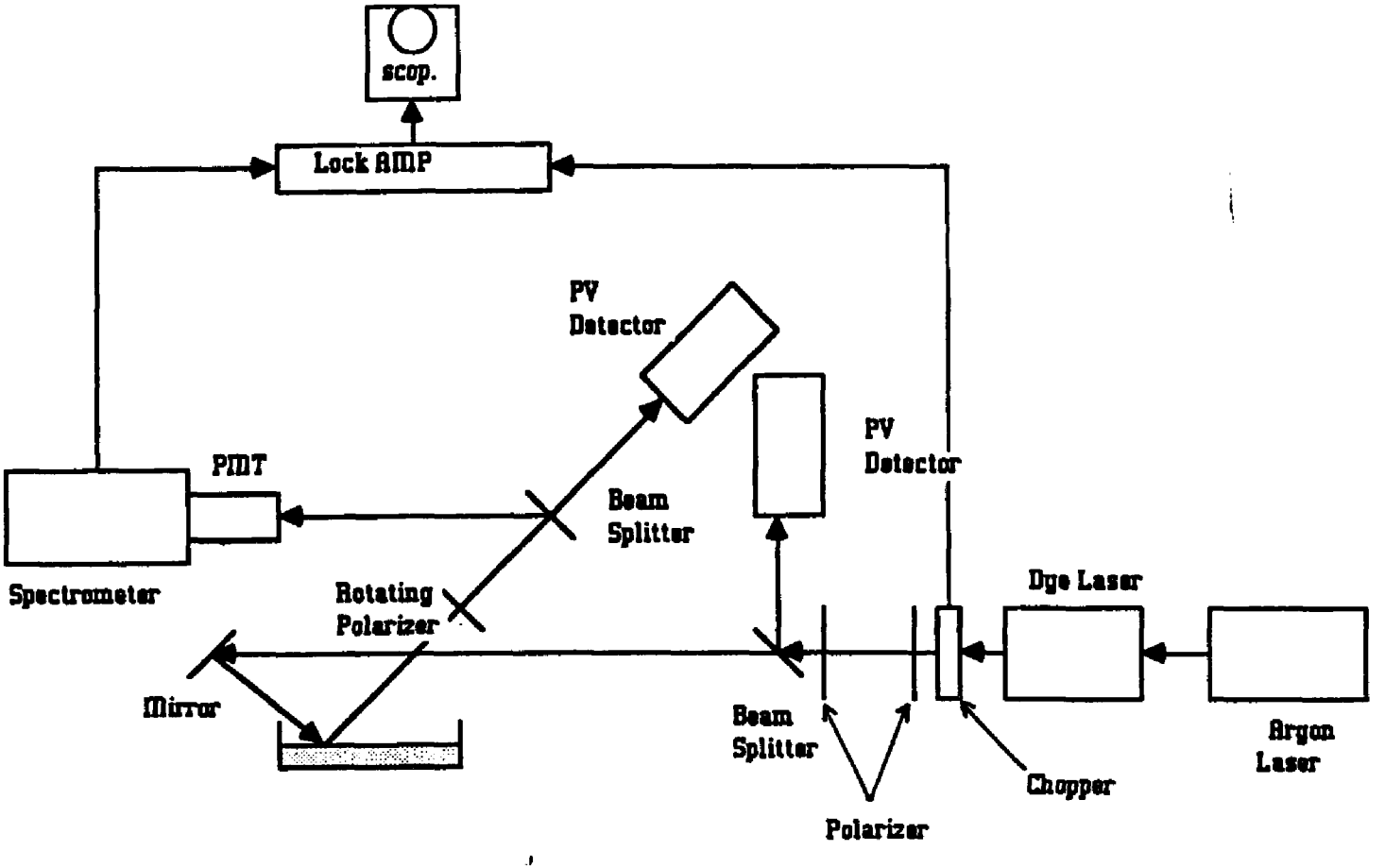

Fig 3.7 Experimental Setup for Depolarization measurement

3.8. COMPARISONS OF THEORETICAL PREDICTIONS AND EXPERIMENTAL RESULTS

The following parameters were measured experimentally and used in the theoretical calculations:

i) an absorption peak (λ_0) at 552 nm,

ii) a line width ($\Delta\lambda$) of approximately 40 nm,

iii) a peak absorption coefficient, α (ω_0) of 5 x 10^4 cm^{-1}.

The arbitrary constant (n_1) in Eq. (3.5.4) is assigned a value of 1.364, which is the refractive index of the solvent (ethanol) used in our experiment. This is understood by assuming a zero value to the absorption coefficient (α) in Eq. (3.5.4), thus the medium is now considered lossless and its refractive index is reduced to the refractive index of the transparent solvent.

Experimental results and their theoretical comparisons are divided into three different sets.

SET I

Experimental measurements were carried out to determine and measure the BP angles as a function of the wavelength, λ.

Fig. 3.8.1 shows the experimental results along with theoretical predictions.

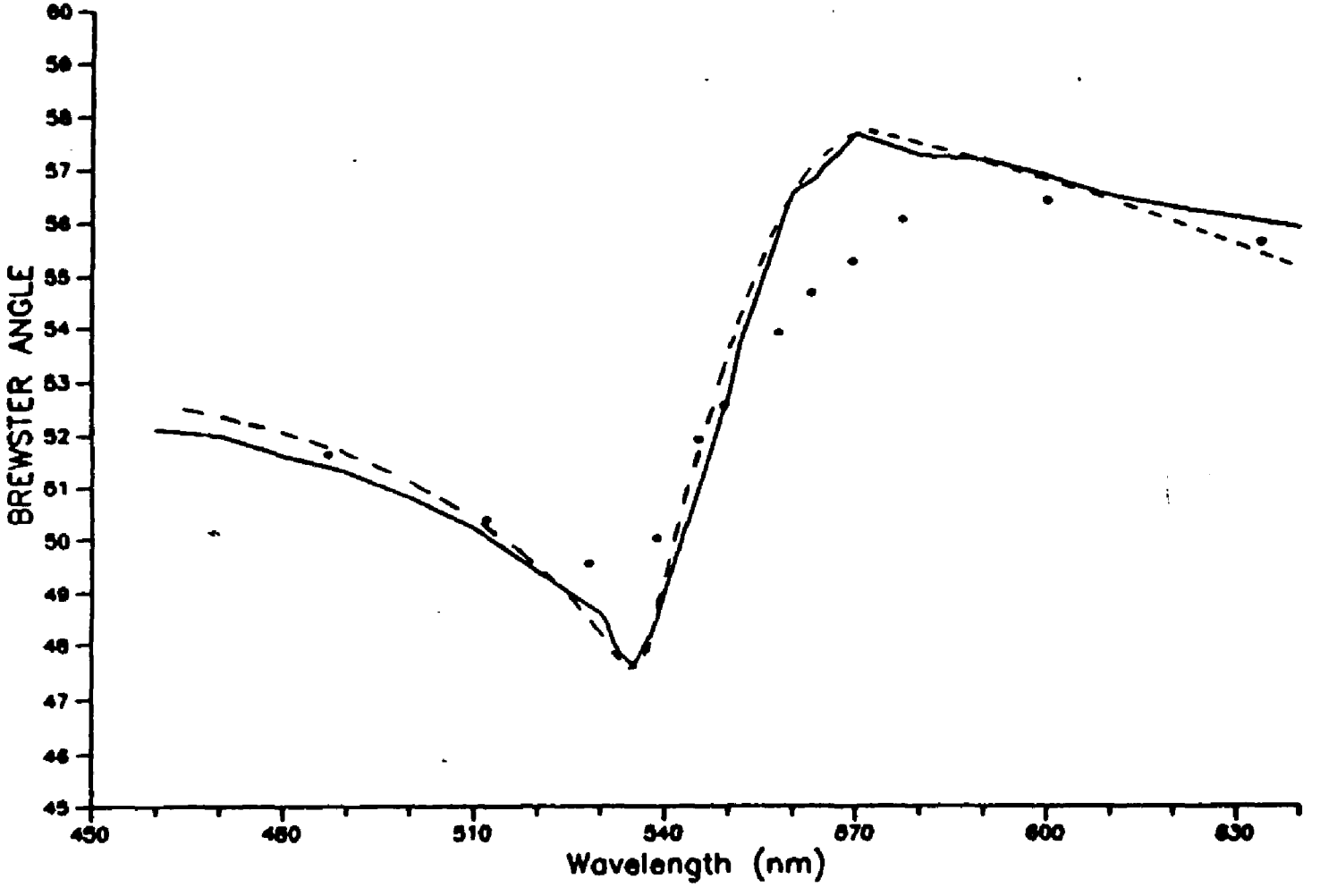

Fig. 3.8.1: Pseudo-Brewster angle ϕ_{PB} vs. λ

____ Theoretical (Lorentzian) ----- Theoretical (actual line shape)

• • • Experimental

The theoretical predictions are made:

(i) using the Lorentzian approximation evaluated, for actual measured values for magnitude of peak absorption, peak wavelength, and the linewidth, and

(ii) by carring out numerical integrations using the actual absorption line shape.

The theoretical predictions are carried out and compared with each other and with the experimental results of this set in Fig. 3.8.1. These comparisons show a good agreement between the Lorentzian approximation and the numerical integration using the actual absorption line shape. Off resonance, where the difference between the Lorentzian line shape and the actual line shape is clear, α has a small value, and R_p values are in general less sensitive to variations in α.

It would be emphasized that, for any given λ, the BP angle was not determined by setting R_p in Eq. (3.4.10) equal to zero and then finding the corresponding angle, since such a solution does not exist. Instead, for a given λ, R_p was calculated for all ϕ's from $\phi = 0 - 90^{\circ}$, with increments of 0.01°, and the angle with corresponding to the minimum reflectance is considered as the BP angle for that λ.

SET II

Theoretical predictions [using Eq. (3.6.4)] and experimental measurements were carried out to determine and measure the fractional depolarization (D) of the reflected beam as a function of the angle of incidence for three different wavelengths, 514 nm, 552 nm, and 580 nm respectively. Figs. 3.8.2, 3.8.3, and 3.8.4 show the theoretical predictions and the corresponding experimental measurements for D vs. the angle of incidence (ϕ) at these wavelengths respectively. Fig. 3.8.2 shows theoretical predictions for both the Lorentzian approximation and the numerical integration using the actual line shape.

With the reasonableness of the Lorentzian approximation established, the remaining figures show only theoretical predictions based on the Lorentzian approximation, along with results of experimental measurements.

From Fig, 3.8.1 we had: at λ= 514 nm, $\phi_{PB} \approx 49^{o}$, at λ= 552 nm, $\phi_{PB} \approx 54^{o}$, and At λ = 580 nm, $\phi_{PB} \approx 57.5^{o}$. It is at these angles in Figs. 3.8.2, 3.8.3, and 3.8.4 respectively where the fractional depolarization, D, is equal one and the reflected beam is totally depolarized.

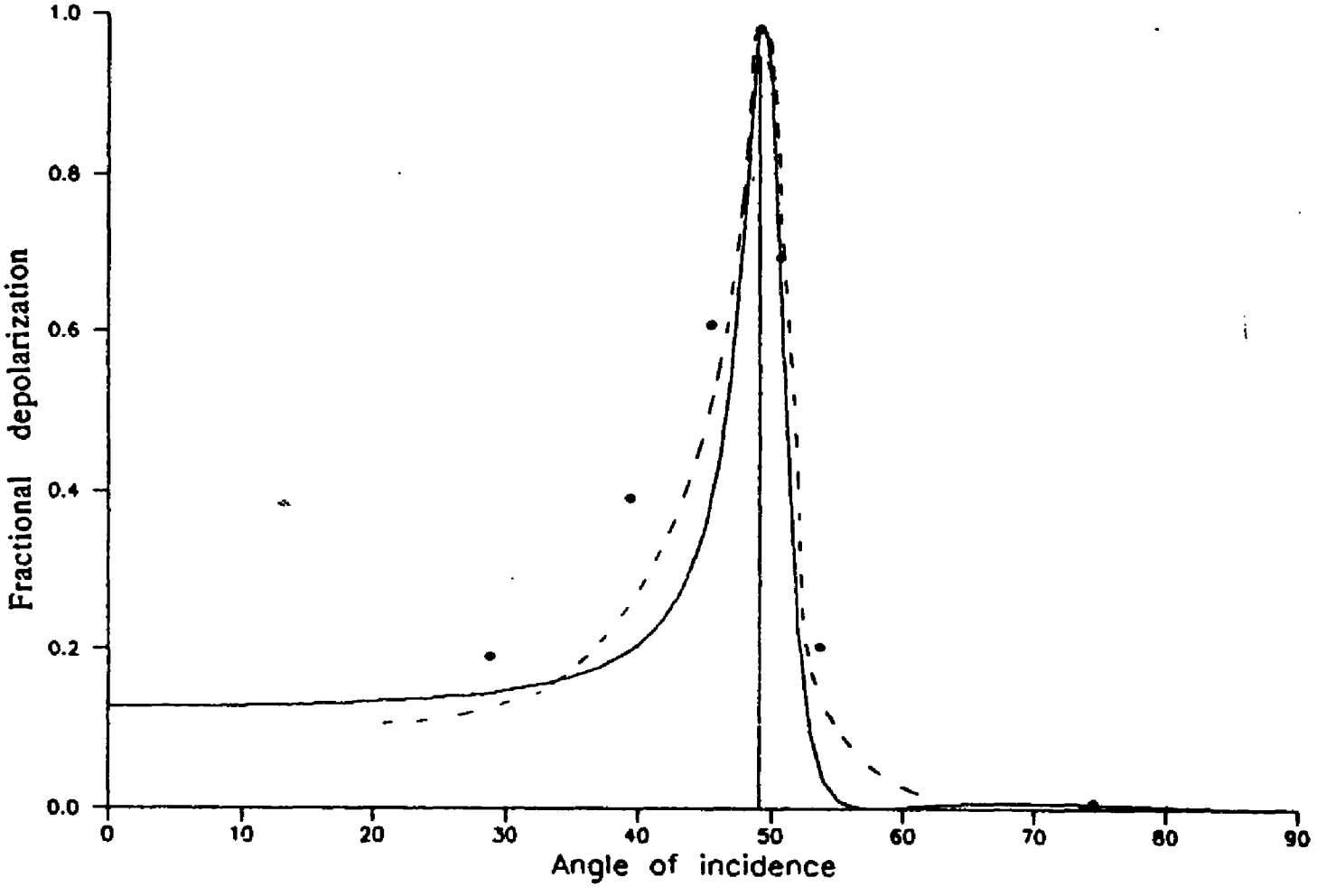

Fig. 3.8.2: Fractional depolarization (D) of the reflected beam vs. angle of incidence ϕ at wavelength λ = 514 n m

____ Theoretical (Lorentzian) ----- Theoretical (actual line shape)

• • • Experimental

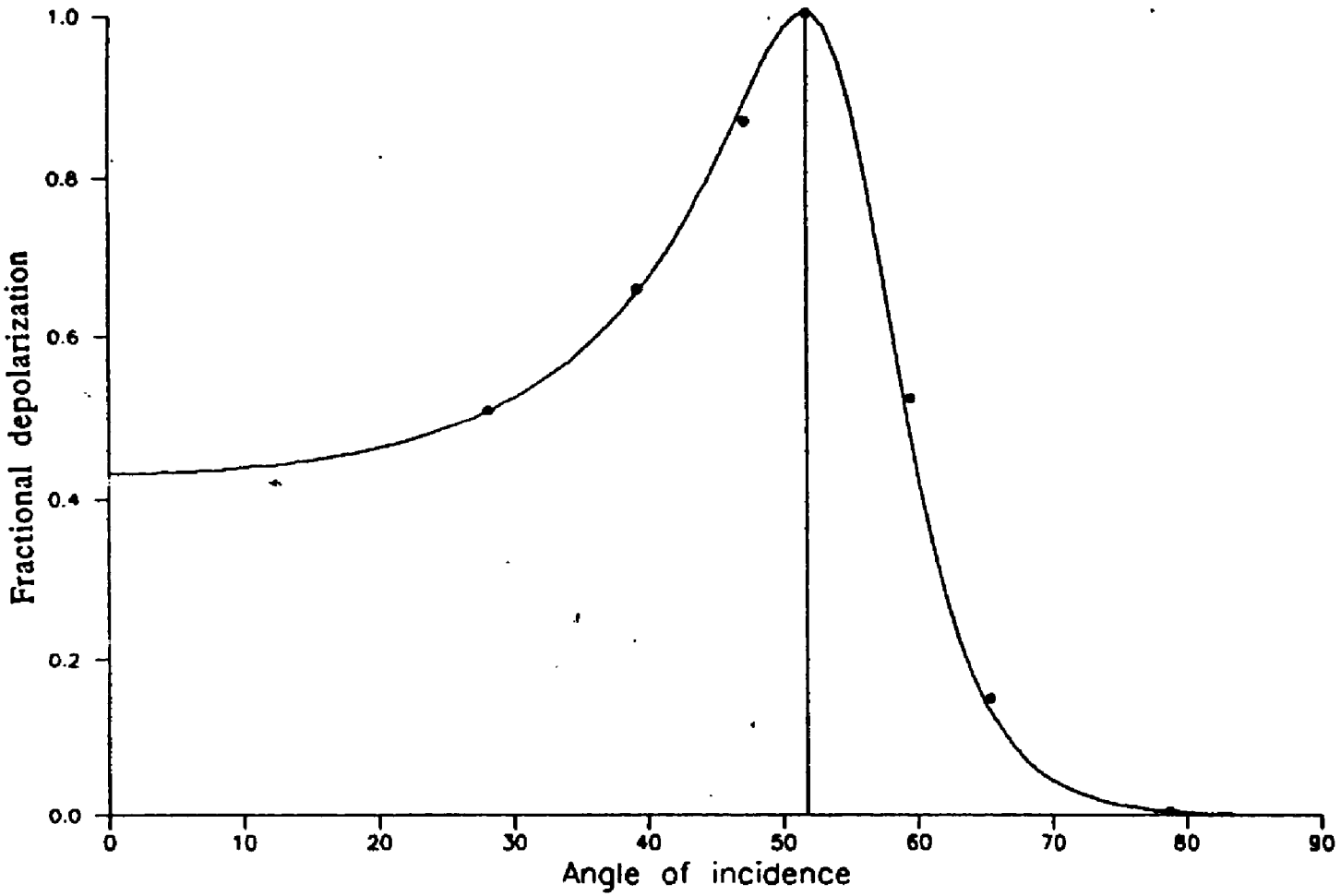

Fig. 3.8.3 : Fractional depolarization (D) of the reflected beam vs. angle of incidence ϕ at wavelength λ = 552 n m

____ Theoretical • • • Experimental

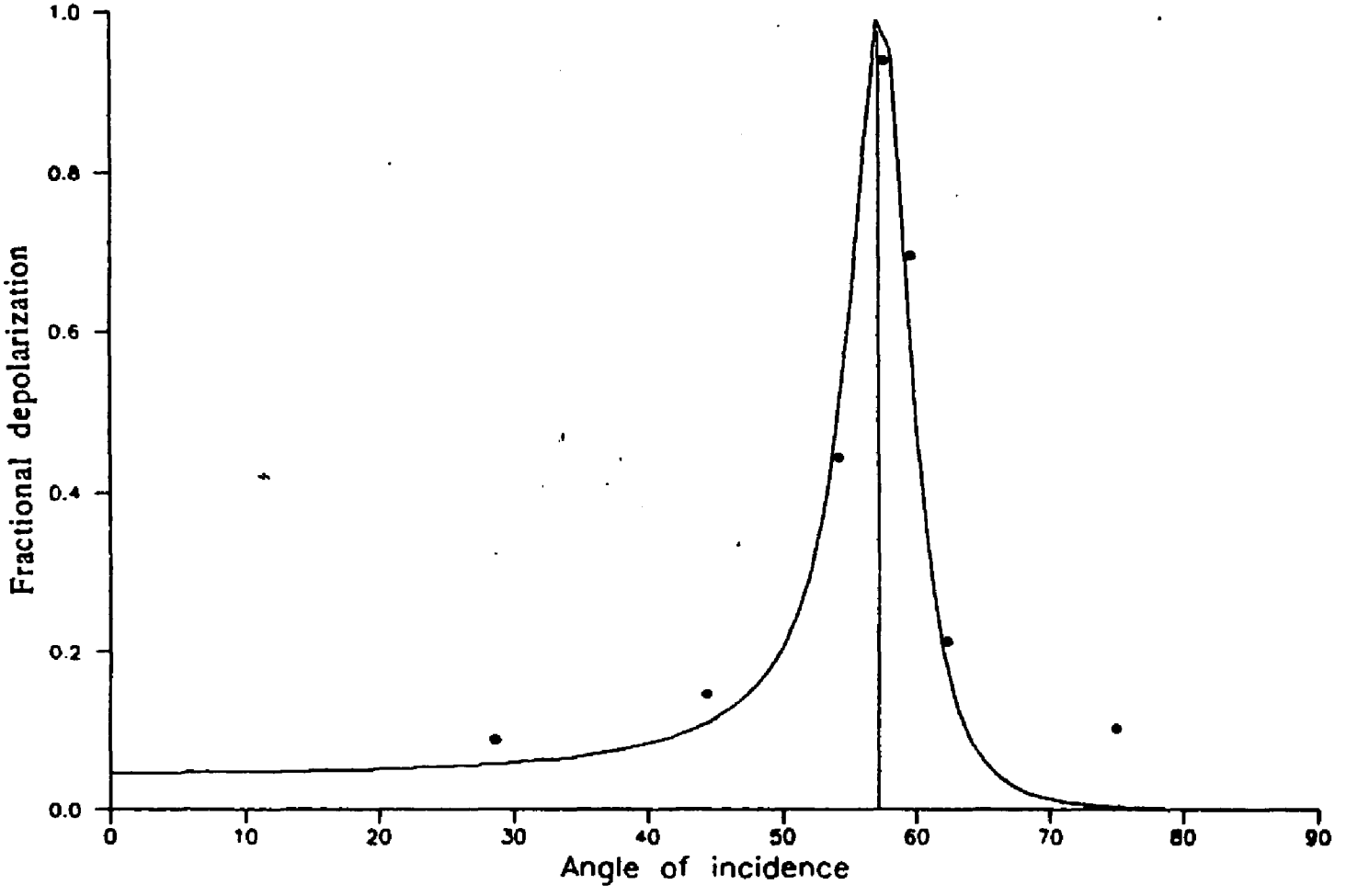

Fig. 3.8.4: Fractional depolarization (D) of the reflected beam vs. angle of incidence ϕ at wavelength λ = 580 n m

____ Theoretical • • • Experimental

SET III

theoretical predictions [using Eq. (3.6.4)] and experimental measurements were carried out to determine and measure the fractional depolarization (D) of the reflected beam as a function of wavelength at three different angles, 29°, 54°, and 75° respectively.

Figs. 3.8.5, 3.8.6, and 3.8.7 show the theoretical predictions and the experimental measurements for D vs. λ at angles 29°, 54°, and 75° respectively. The significance of choosing the angle 54° is that, this is the PB angle at the resonance frequency (552 nm) where D is expected to be one (Fig. 3.8.6).

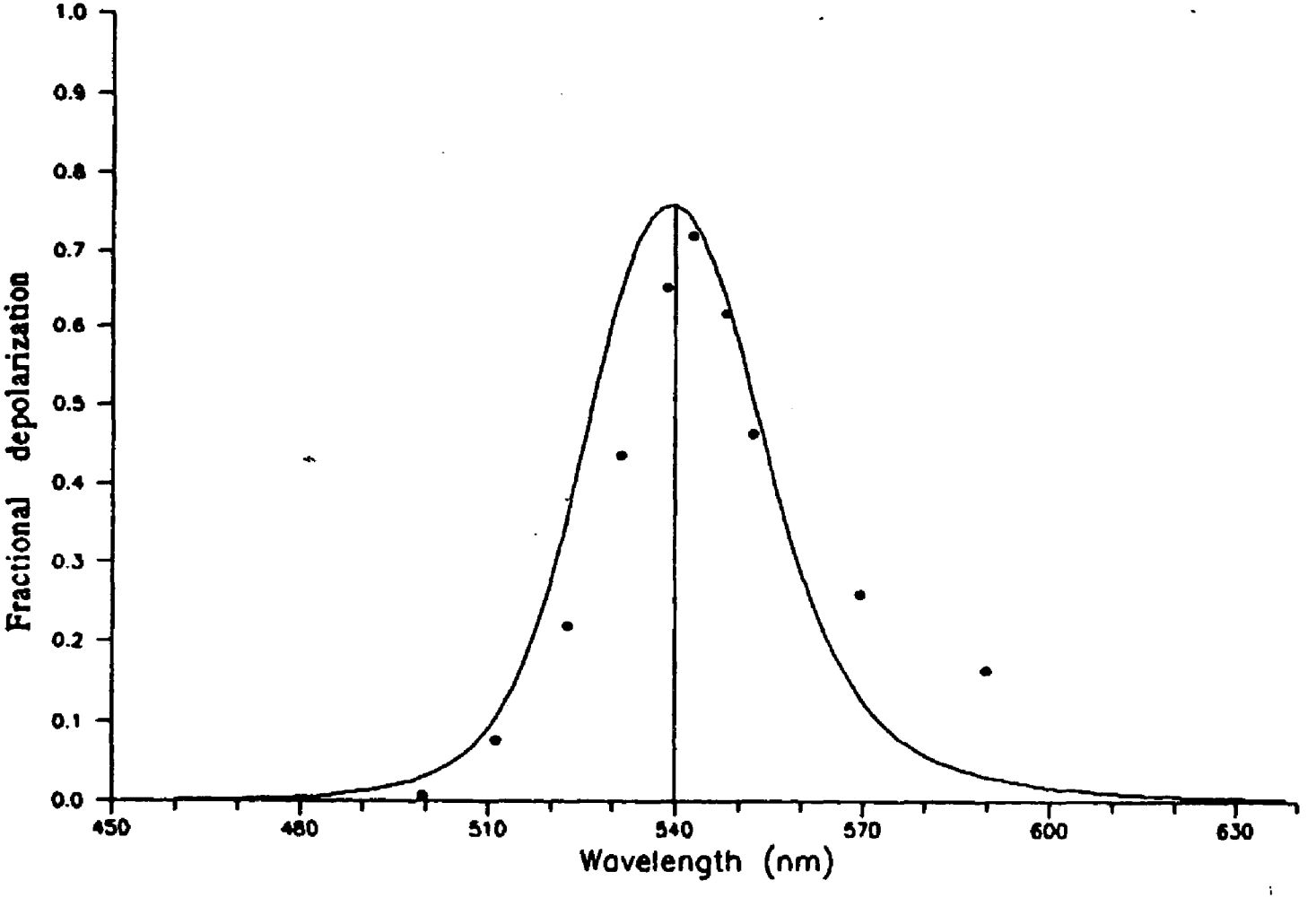

Fig. 3.8.5 : Fractional depolarization (D) of the reflected beam vs. λ for Rh B solution at angle of incidence $\phi = 29^{o}$

——— Theoretical • • • Experimental

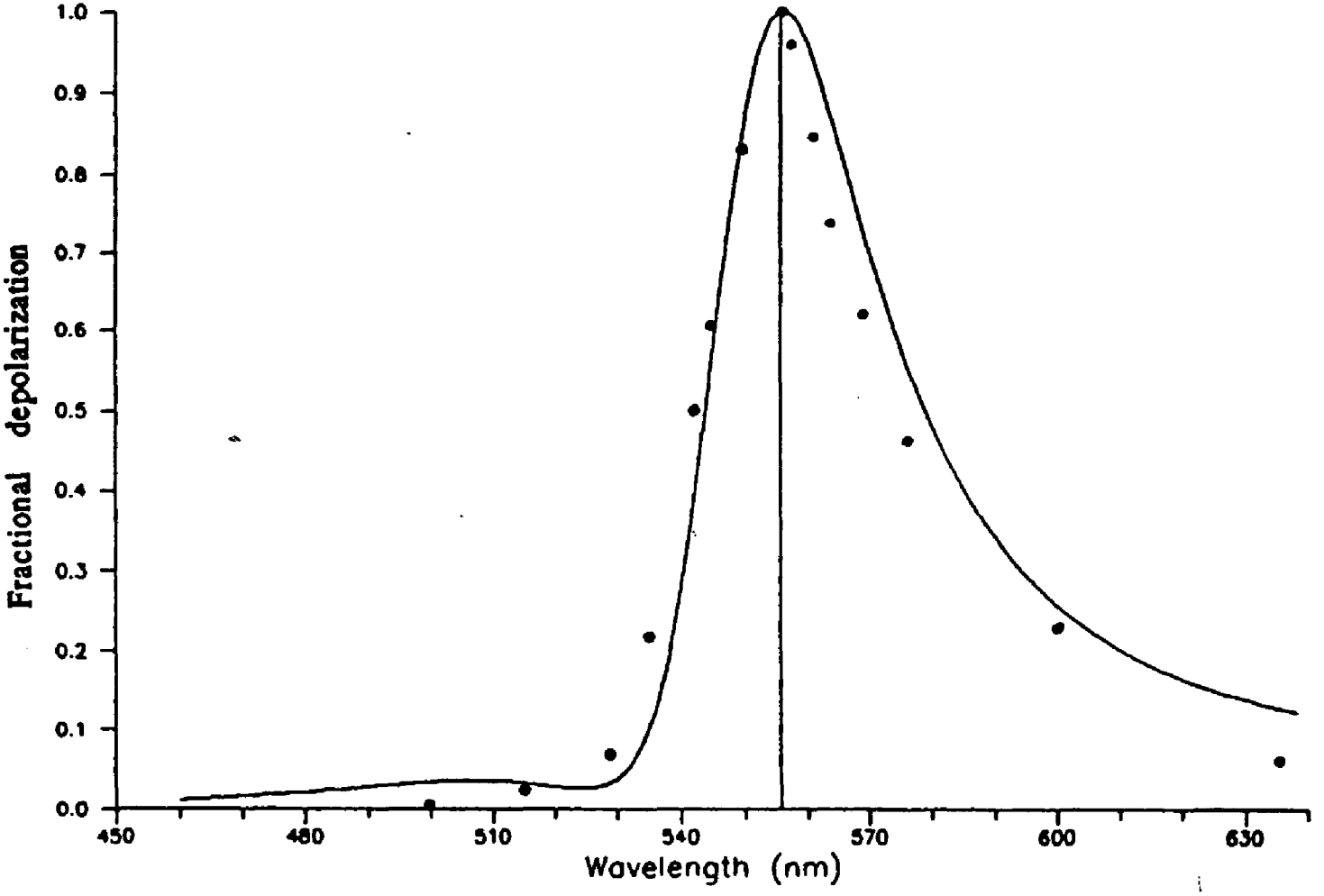

Fig. 3.8.6: Fractional depolarization (D) of the reflected beam vs. λ for Rh B solution at angle of incidence $\phi = 54^{o}$

——— Theoretical • • • Experimental

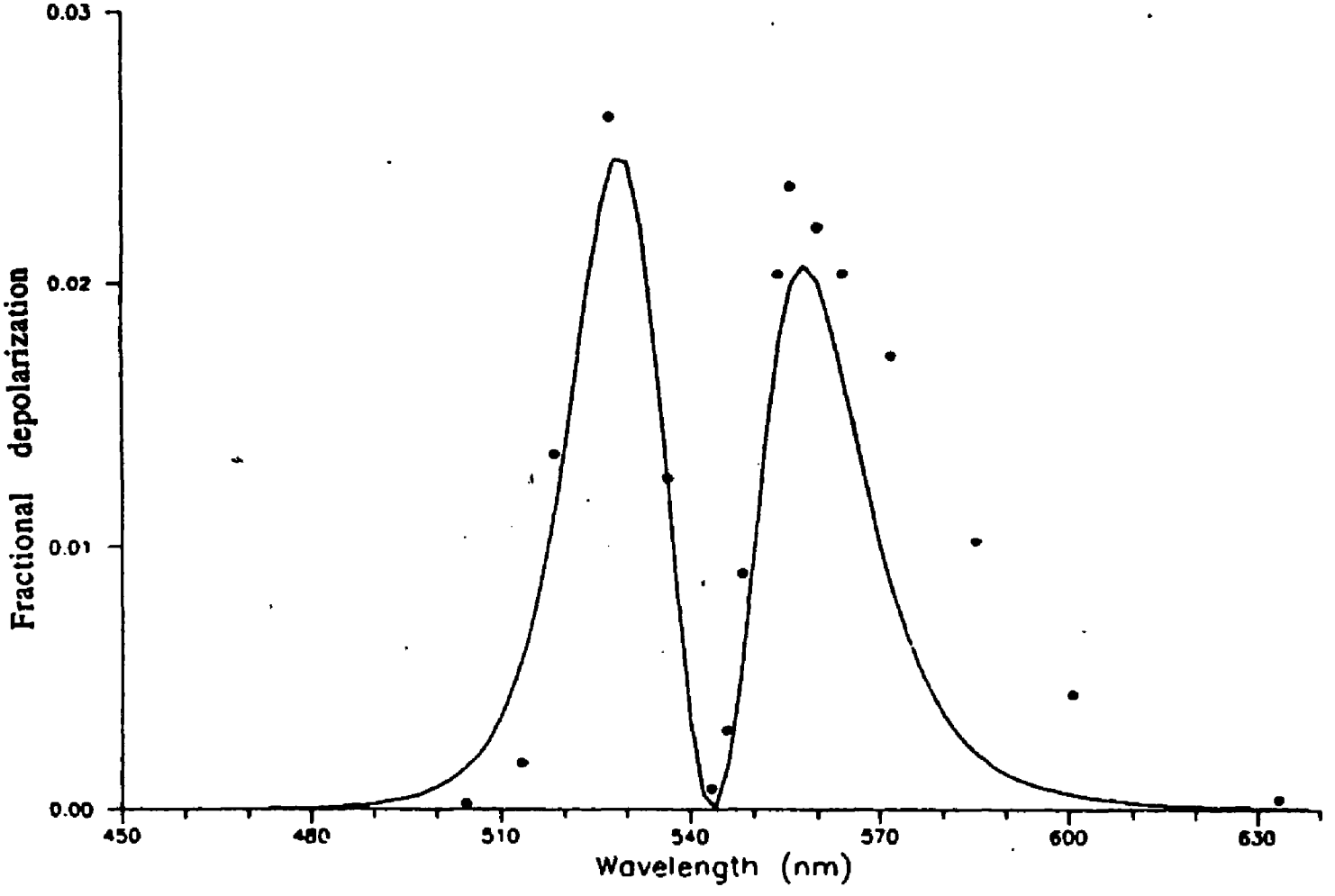

Fig. 3.8.7: Fractional depolarization (D) of the reflected beam vs. λ for Rh B solution at angle of incidence $\phi = 75^{o}$

____ Theoretical • • • Experimental

Summing up, it was found that, at all the PB angles for all wavelengths of interest, the reflected beam is totally depolarized (in a direction normal to the plane of incidence i.e. it represents the component of the specular reflection perpendicular to the plane of incidence, R_s) explaining why R_p never drops to zero at the PB angles.

Appendix A:

$$r_p = \frac{\epsilon \cos\phi - (\epsilon - \sin^2\phi)^{1/2}}{\epsilon \cos\phi + (\epsilon - \sin^2\phi)^{1/2}}$$

$$r_s = \frac{\cos\phi - (\epsilon - \sin^2\phi)^{1/2}}{\cos\phi + (\epsilon - \sin^2\phi)^{1/2}} \qquad (A.1)$$

where p and s identify the linear polarizations parallel and perpendicular to the plane of incidence, respectively. ϕ is angle of incidence, and $\varepsilon = \varepsilon_1 / \varepsilon_o$ is the complex ratio of dielectric constants of the two media defined as:

$$\varepsilon = \varepsilon' + j\varepsilon''$$

and rewritten for algeberiac convenience as: (A.2)

$$\varepsilon = a + jb$$

substituting Eq. (A.2) into Eq. (A.1) for the case of parallel polarization gives,

$$r_p = \frac{(a+jb)\cos\phi - (a+jb - \sin^2\phi)^{1/2}}{(a+jb)\cos\phi + (a+jb - \sin^2\phi)^{1/2}} \qquad (A.3)$$

let

$$Q = a - \sin^2 \phi, \qquad |U| = (Q^2 + b^2)^{1/2},$$

$$\theta = \tan^{-1}(b / Q) \qquad Z = \sqrt{|U|} / \cos \phi$$

then, Eq. (A.3) can be rewritten in the form:

$$r_p = \frac{(a + jb) - Z \exp\{j\theta / 2\}}{(a + jb) + Z \exp\{j\theta / 2\}} \qquad (A.4)$$

or:

$$r_p = \frac{\{a - Z\cos(\theta / 2)\} + J\{b - Z \sin(\theta / 2)\}}{\{a + Z\cos(\theta / 2)\} + J\{b + Z \sin(\theta / 2)\}} \qquad (A.5)$$

if we further define:

$$\Omega_1 = a - Z\cos(\theta / 2)$$
$$\Omega_2 = a + Z\cos(\theta / 2)$$
$$\beta_1 = b - Z\sin(\theta / 2)$$
$$\beta_2 = b + Z\sin(\theta / 2) \qquad (A.6)$$

then Eq. (A.5) can be written as:

$$r_p = \frac{\Omega_1 + j\beta_1}{\Omega_2 + j\beta_2} \qquad \text{(A.7)}$$

or equivalently

$$r_p = \left\{ \frac{\Omega_1\Omega_2 + \beta_1\beta_2}{\Omega_2^2 + \beta_2^2} \right\} + J\left\{ \frac{\beta_1\Omega_2 - \beta_2\Omega_1}{\Omega_2^2 + \beta_2^2} \right\} \qquad \text{(A.8)}$$

Appendix B:

Consider $\oint_c F(\omega)\,d\omega$ where C is the closed contour shown in Fig. 10 and F(w) is given by:

$$F(\omega) = \frac{d\omega}{\omega(\omega - \omega')\left\{(\omega - \omega_o)^2 + \gamma^2\right\}} \tag{1}$$

integrating the function F(ω) over the contour shown:

$$\oint_C F(\omega)\,d\omega = \int_{-R}^{-\epsilon} F(\omega)d\omega + \int_{c_1} F(\omega)d\omega + \int_{\epsilon}^{\omega'-\epsilon} F(\omega)d\omega + \int_{c_2} F(\omega)d\omega + \int_{\epsilon+\omega'}^{R} F(\omega)d\omega + \int_{c_3} F(\omega)d\omega \tag{2}$$

where c_1, c_2, and c_3 are the semicircular arcs of radii, ε, ε, and R.

we next take the limit of Eq. 2 as $R \to \infty$ and $\epsilon = 0$

The integral over C3 vanishes for $F(\infty) \to 0$ while the integral over C becomes:

$$\frac{-\pi}{\gamma(\omega_o + i\gamma)(\omega' - \omega_o - i\gamma)} = \text{P.V.} \int_{-\infty}^{\infty} F(\omega)d\omega + \frac{i\pi}{\omega'(\omega_o^2 + \gamma^2)} - \frac{i\pi}{\omega'\left\{(\omega' - \omega_o)^2 + \gamma^2\right\}} \tag{3}$$

where:

$$\frac{-\pi}{\gamma(\omega_o + i\gamma)(\omega' - \omega_o - i\gamma)} = 2\pi i \text{ (residue) of } F(\omega) \text{ at } \omega = \omega_o + i\gamma = \text{L.H.S. of Eq.2}$$

$$\frac{i\pi}{\omega'\left(\omega_0^2+\gamma^2\right)} = \int_{C_1} F(\omega)d\omega = -\,i\pi \text{ (residue) of } F(\omega) \text{ at } \omega = 0$$

$$\frac{-\,i\pi}{\omega'\left\{\left(\omega'-\omega_0\right)^2+\gamma^2\right\}} = \int_{C_2} F(\omega)d\omega = -\,i\pi \text{ (residue) of } F(\omega) \text{ at } \omega = \omega'$$

from Eq. 3 we get:

$$\text{P.V.} \int_{-\infty}^{\infty} F(\omega)d\omega = \frac{\pi\left\{\omega_0^2-\omega_0\omega'-\gamma^2\right\}}{\gamma\left(\omega_0^2+\gamma^2\right)\left\{\left(\omega'-\omega_0\right)^2+\gamma^2\right\}} \tag{4}$$

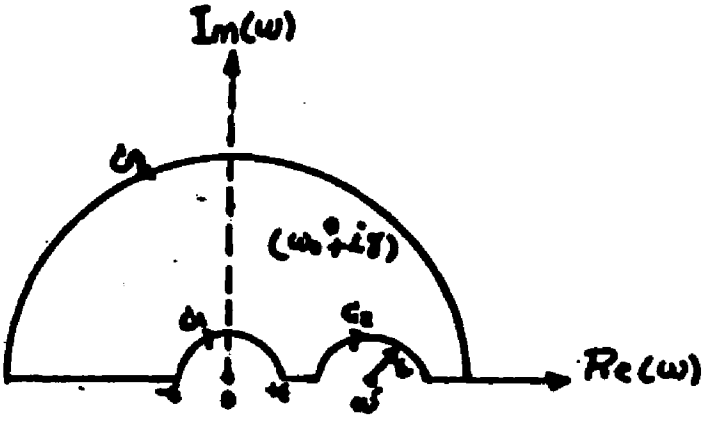

Fig. A.1: The integration contour used to derive the real part (n) of the complex refractive index (N)

References

[1] David L. Greenaway and G. Harbeke, Optical properities and band structure of semiconductors, Pergamon press, New York, 1968.

[2] H. R. Philipp and E. A. Taft, Optical Constants of Germanium in the Region 1 to 10 ev, Phys. Rev. 113, 1002 (1959).

[3] Edward D. Palik, Handbook of Optical Constants of Solids, Academic Press, New York, 1985.

[4] S. P. F. Humphreys-Owen, Comparison of Reflection Methods for Measuring Optical Constants, Proc. Phys. Soc. (London) 77, 949 (1961).

[5] D. E. Aspnes, and A. A. Studna, Dielectric Functions and Optical Parameters of Si, Ge, GaP, GaAs, GaSb, InP, InAs, and InSb from 1.5 to 6.0 ev, Phys. Rev. B 27, 985 (1983)

[6] R. M. A. Azzam and N. M. Bashara, Ellipsometry and Polarized Light (North-Holand, Amsterdam, 1977)

[7] F. C. Jahoda, Fundamental Absorption of Barium Oxide from Its Reflectivity Spectrum, Phys. Rev. 107, 1261 (1957).

[8] H. R. Philipp and E. A. Taft, Optical Constants of Silicon in the Region 1 to 10 ev, Phys. Rev. 120, 37 (1960).

[9] H. R. Philipp and E. A. Taft, Optical Properties of Diamond in the Vacuum Ultraviolt, Phys. Rev. 127, 159 (1962).

[10] R. M. A. Azzam and A. M. El-Saba, Applied Optics, 27, No. 19, 1988.

[11] Amon Yariv, Quantum Electronics, Wiley, New York, 1975.

[12] W. R. Hunter, J. Optical Soc. Am. 55, 1197(1965)

[13] G. R. Field and E. Murphy, Appl. Opt. 10, 1402 (1971)

[14] Barry S. Gourary, J. Applied Phys., 28, 3, 1957.

[15] J. H. Van Vleck, Atomspheric Attenuation, Rl Report No. 735, (1945).

[16] H. A. Kramers, Atti cong. intern. fisici, Como, 2 545 (1927)

[17] D. S. Kokkinos, LIDAR System Using Polarization Discrimination Techniques for Molecular Air Pollution Monitoring, 1984.